Article

Experimental Optimization with the Emphasis on Techno-Economic Analysis of Production and Purification of High Value-Added Bioethanol from Sustainable Corn Stover

Sara E. AbdElhafez [1], Tarek Taha [2], Ahmed E. Mansy [3], Eman El-Desouky [4], Mohamed A. Abu-Saied [5], Khloud Eltaher [4], Ali Hamdy [2], Gomaa El Fawal [5], Amr Gamal [6], Aly M. Hashim [7], Abdallah S. Elgharbawy [8,9], Mona M. Abd El-Latif [1], Hesham Hamad [1,10,*] and Rehab M. Ali [1,*]

[1] Fabrication Technology Research Department, Advanced Technology and New Materials Research Institute (ATNMRI), City of Scientific Research and Technological Applications (SRTA-City), New Borg El-Arab City 21934, Alexandria, Egypt
[2] Environmental Biotechnology Department, Genetic Engineering and Biotechnology Research Institute (GEBRI), City of Scientific Research and Technological Applications (SRTA-City), New Borg El-Arab City 21934, Alexandria, Egypt
[3] Environment and Natural Materials Research Institute (ENMRI), City of Scientific Research and Technological Applications (SRTA-City), New Borg El-Arab City 21934, Alexandria, Egypt
[4] Chemistry Department, Faculty of Science, Alexandria University, Ibrahimia 21321, Alexandria, Egypt
[5] Polymeric Materials Research Department, Advanced Technology and New Materials Research Institute (ATNMRI), City of Scientific Research and Technological Applications (SRTA-City), New Borg El-Arab City 21934, Alexandria, Egypt
[6] Physics Department, Faculty of Science, Alexandria University, Moharam Bek 21568, Alexandria, Egypt
[7] Central Laboratory, City of Scientific Research and Technological Applications (SRTA-City), New Borg El-Arab City 21934, Alexandria, Egypt
[8] Materials Science Department, Institute of Graduate Studies and Research (IGSR), Alexandria University, Shatby 21526, Alexandria, Egypt
[9] The Egyptian Ethylene and Derivatives Company (ETHYDCO), Ameriya 23511, Alexandria, Egypt
[10] Faculty of Chemistry, University of Warsaw, Pasteur 1, 02-093 Warsaw, Poland
[*] Correspondence: heshamaterials@hotmail.com or hhamad@srtacity.sci.eg (H.H.); rehabmohamedali1983@gmail.com or rali@srtacity.sci.eg (R.M.A.); Tel.: +20-12-75026292 (H.H.); +20-12-23810108 (R.M.A.)

Abstract: Bioethanol-derived biomass is a green sustainable source of energy that is highly recommended as an efficient alternative to the replacement of fossil fuels. However, this type of bioethanol production is always expensive with very low bioethanol concentration. Therefore, this work aims to represent a facile and green approach for bioethanol production with high concentration and purity as well as reasonable cost from corn stover (CS). The goal of this study is to characterize CS and its treated samples with maleic acid (CSM) using various characterization analyses, such as proximate and ultimate analysis, HHV, TGA, FTIR, SEM, and CHNS. The bioethanol production stages: Pretreatment, enzymatic degradation, fermentation, and finally bioethanol separation and purification via the pervaporation process, which have been investigated and optimized are associated with the economic analysis. The optimum operating condition of the pretreatment process was 2% maleic acid, 1:20 solid-to-liquid ratio at 45 psi, 120 °C, and 1 h of operation in the autoclave. This process contributes to 53 and 45% lignin and hemicellulose removal, 98% cellulose recovery, and a glucose yield of 741 mg/dL. The yeast isolate succeeded in the production of 1230 mg/dL of bioethanol. This isolated yeast strain was close to *Pichia nakasei* with a similarity of 98%, and its amplified 18S rRNA gene sequence was deposited in GenBank with the accession number MZ675535. Poly (MMA-*co*-MA) membrane was synthesized, characterized, and its efficiency for increasing the bioethanol concentration was evaluated using the integrated pervaporation technique. The techno-economic analysis is presented in detail to evaluate the process profitability, which achieves a considerable profit for the whole duration of the project without any losses as it reaches a net profit of USD 1 million in 2023, reaching USD 2.1 million in 2047 for a company with a capacity of 32 thousand tons per year. The sequential strategy offers a promising approach for efficient bioethanol production under mild and environmentally friendly conditions that enable its implication industrially.

1. Introduction

Biomass energy, which is the most notable sustainable source of energy, has attracted global attention in recent years to solve the intractable problems of accelerated energy consumption rates, fast diminishing fossil fuels, and the environmental pollution issues generated from fossil fuel consumption [1]. The annual biomass energy contributes 45 ± 10 exajoules to the world's energy supply, which includes modern uses (e.g., liquid biofuels for producing electricity and steam) and traditional uses (e.g., burning for heating and cooking) [2]. Biomass energy is a renewable source of energy that is derived from animals, plants, and organic materials and used as feedstock for biodiesel and bioethanol green sustainable production.

Bioethanol has a high-octane number compared with gasoline, and it is used as a brilliant alternative energy source [3]. Bioethanol production from lignocellulosic biomass reduces greenhouse gas emissions since it is considered as atmospheric carbon-neutral. Therefore, there is no change in the net emissions of carbon dioxide (CO_2) using bioethanol as a source of energy [4]. Moreover, the average global warming potential (GWP) of bioethanol is lower than petrol ethanol (23–59 vs. 94 g CO_2 eq. MJ^{-1}) [5]. As a result, replacing petrol ethanol with bioethanol can reduce the extensive emissions of CO_2, in addition to avoiding open biomass burning that increases the CO_2 emissions. Furthermore, bioethanol production from lignocellulosic biomass leads to a more sustainable future as it is available, renewable, decreases the dependency on imported fuels, leads to agricultural development, achieves energy security, increases investment in plant and equipment, as well as increases the number of rural manufacturing jobs [6].

Corn stover (CS) is a strategic crop and widely produced biomass of high lignocellulose content that can be utilized as biomass feedstock for bioethanol production. The CS composition ranges are hemicellulose (19–27%), cellulose (32–47%), and lignin (5–24%). Hemicellulose is the polysaccharide of C5, and C6 sugars and acids can hydrolyze it to monomer components, such as xylose (14.8–20.2%), glucose (41–43.4%), arabinose (2.7–4.5%), mannose (1.8%), and galactose (0.4%) [7]. Bioethanol production from CS depends on four major operations: Pretreatment, hydrolysis, fermentation, and purification. The first operation (pretreatment) is critical to facilitate the enzyme accessibility to the cellulose and hemicellulose by reducing cellulose crystallinity, increasing cellulose fractionation, increasing materials porosity, and disrupting the lignocellulosic complex by removing lignin. This is strongly linked with hemicelluloses and celluloses (carbohydrates) through hydrogen and covalent bonds that make the structure identical in robustness and complexity [8].

The pretreatment process has been extensively developed using mineral acids, alkalis, organic acids, or inorganic salts to achieve maximum lignin and hemicellulose removal and cellulose recovery. Chen et al. utilized dilute H_2SO_4 that led to 12.2 and 76.6% lignin and hemicellulose removal from corn stover and 95.5% cellulose recovery. The use of lime led to 34.8 and 14.8% lignin and hemicellulose removal and 93.2% cellulose recovery. The CS was pretreated using ammonia/HCl, which led to 41 and 67.8% lignin and hemicellulose removal and 91.1% cellulose recovery [9]. Tan et al. investigated the effect of peracetic acid on the lignocellulosic structure and reported that peracetic acid led to 97% lignin removal [10]. Elyamny et al. utilized $ZnCl_2$ for the pretreatment of CS, which led to 32% lignin removal and 98.7% cellulose recovery. The use of combined Na_2HPO_4 and $ZnCl_2$ led to 37% lignin removal and 99.75% cellulose recovery [6].

Although mineral acids, such as HCl, H_2SO_4, or H_3PO_4, are widely used for breaking down the lignocellulosic structure and cellulose fractionation, it has many drawbacks, such as equipment corrosion, reducing the industrial installations lifetime, consuming

high energy and chemical cost, formation of inhibitory compounds such as furfurals and 5-(hydroxymethyl)furfural that affect the fermentation process, as well as generating toxic by-products for downstream use that lead to environmental pollution [11–13]. Moreover, the pretreatment process has been investigated using alkalis, such as NaOH and ammonia. However, the NaOH pretreatment generates black liquor, which leads to environmental pollution. Furthermore, the ammonia pretreatment has no adverse environmental impacts, but it is not sufficient for the efficient pretreatment and delignification process [12]. The advantage of using dilute organic acid pretreatment processes is the high lignin removal without breaking down cellulose. Moreover, it produces high glucose yields that are fermented easily and produce high bioethanol concentrations [14]. Yan et al. proved that maleic acid is a promising organic acid that provides selective hemicellulose hydrolysis and lignin removal, less sugar degradation, and higher sugar yield compared with dilute sulfuric acid, controls stepwise acidity, and causes limited corrosion compared with mineral acids [15].

The bioethanol purification from fermentation broth is typically accomplished through distillation, which is a complex and energy-intensive process. It is estimated that the distillation process consumes more than half of the total energy consumed in bioethanol production [16]. Pervaporation (PV) is a non-distillation method for bioethanol recovery from fermentation. It is a purification technique that is regarded as a viable alternative to traditional techniques of organic mixtures separation as a result of its great accuracy, low energy cost, and lack of negative effects on microorganisms. It is performed by changing the diffusivity and solubility of the ingredients for isolation by a tightly packed membrane. Therefore, organophilic (hydrophobic) membranes are the main component of PV technology. Numerous membranes have been extensively studied, such as poly (1-trimethylsilyl-1-propyne) (PTMSP), poly (ether-block-amide) (PEBA), and polydimethyl-siloxane (PDMS). The PEBA, which contains hard polyamide and soft polyether (PE) that are combined with no cross-linking, can be used as efficient membranes for the separation of organic solvents [17]. Many studies are searching for unique membranes to separate ethanol, such as polymer blends, homopolymers, copolymers, and modified polymers [18].

According to the aforementioned information, the purpose of the current study is to optimize the overall operating conditions to produce the optimum bioethanol concentration with the highest purity and lowest production cost. The pretreatment stage was performed using various organic acids to compare their effects on delignification, hemicellulose removal, and cellulose fractionation. The acid that led to the highest delignification would be selected for the pretreatment process. In addition, the parameters affecting the CS pretreatment, such as autoclaving time, acid concentration, solid-to-liquid ratio, and temperature have been investigated and optimized to produce the optimum glucose concentration, as well. To optimize the bioethanol overall process, the enzymatic degradation process and the fermentation process parameters have been investigated to produce the optimum bioethanol concentration. For efficient bioethanol separation, increasing the bioethanol concentration, and producing bioethanol with high purity, poly (methyl methacrylate-*co*-methyl acrylate) (poly (MMA-*co*-MA)) membrane was synthesized, characterized, and subjected to a pervaporation system. Moreover, the study analyzes, evaluates, and compares the influence of different ethanol concentrations on membrane flow and selectivity in the binary feed mixture. Furthermore, the diffusion coefficient and pervaporation results have been interpreted based on the principles of solution-diffusion. Finally, an economic analysis has been investigated to provide an overall view of the bioethanol production process feasibility and profits based on the optimum operating condition obtained from the experimental work. A summary of the sequence of the bioethanol production process stages from CS and the studied parameters have been described in Figure 1.
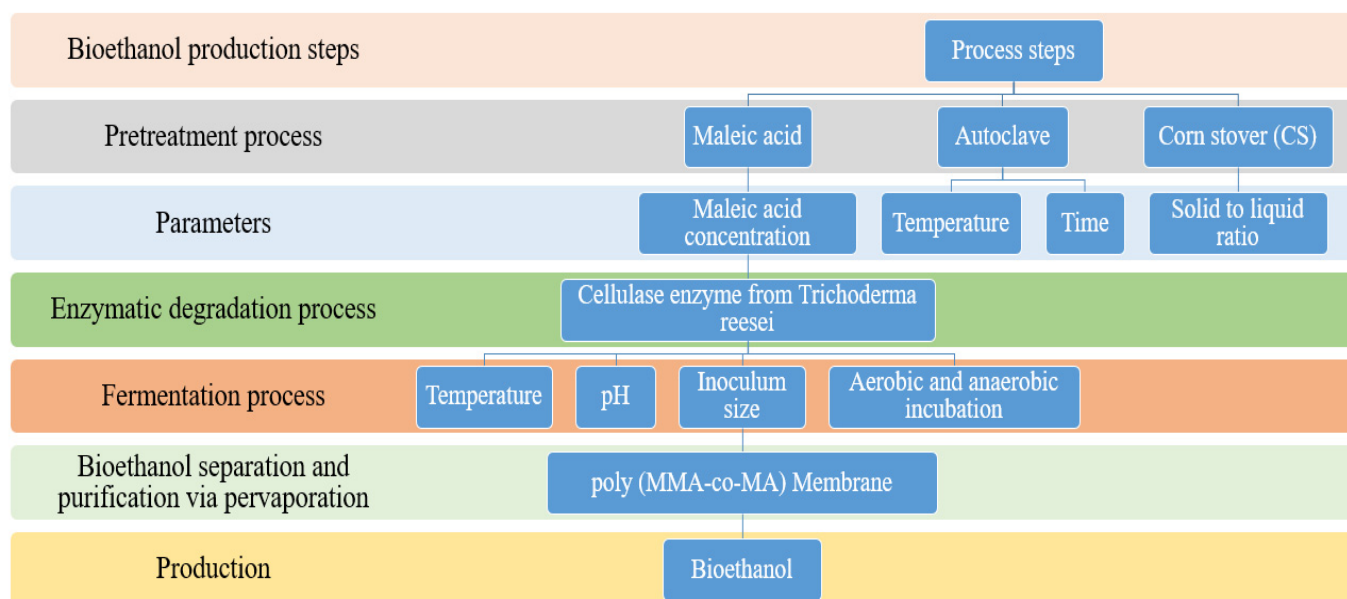
Figure 1. Schematic diagram of bioethanol production stages from CS.

2. Materials and Methods

2.1. Biomass and Chemicals

The CS was collected from Beheira and Alexandria farms, Egypt. Maleic acid, oxalic acid, succinic acid, and lactic acid were supplied by Serva electrophoresis GmbH, Heidelberg, Germany. Cellulase enzyme from *Trichoderma reesei* ($\geq$700 U/g) was supplied by Sigma-Aldrich, Søborg, Denmark. The other chemicals of the pretreatment process were of analytical grade and supplied by Sigma-Aldrich. Absolute ethanol and sulfuric acid HPLC grades were supplied by Fisher Scientific, Loughborough, UK. Poly (MMA-*co*-MA) membrane was supplied by Polysciences Company, Tamil Nadu, India, with an average molecular weight of around 34 thousand g/mole. N, N dimethylformamide (DMF) was supplied by Panreac, Barcelona, Spain.

2.2. Biomass Elaboration

The biomass was washed twice with tap water to remove the dust and dirt. The washed biomass was dried at 60 °C for 48 h until constant weight, crushed, and sieved through a 100-mesh screen (Retsch, AS200, Haan, Germany). The prepared materials were stored dry at room temperature in sealed bags for further pretreatment and analysis.

2.3. Physico-Chemical Pretreatment and Cellulose Fractionation

The pretreatment process was conducted by applying mutual chemical and physical pretreatment. To increase the chemical pretreatment efficiency, heating using a pressurizing source (autoclave) is applied as a physical pretreatment to enhance the lignin and hemicelluloses degradation and increase enzymatic susceptibility [19]. In this process, four autoclavable vessels were prepared, in each one, a 10 g biomass sample was loaded with 100 mL of 2% of various organic acids (maleic acid, oxalic acid, succinic acid, and lactic acid) solutions and these pretreated samples were labeled as CSM, CSO, CSS, and CSL, respectively. The mixture was located in an autoclave at 3.1 bars, 120 °C for 60 min residence time.

To investigate the optimum physico-chemical pretreatment operating conditions, various CSM substrates to liquid ratios of 1:10, 1:20, 1:30, 1:40, and 1:50 were conducted, while the acid concentration was varied from 1 to 7%. The effect of the autoclaving time was investigated from 10 to 120 min. Each experiment was individually added to 5 mL acetate buffer (pH 5.5) in separated tubes. Each tube was amended with 100 µL of the cellulase enzyme followed by incubation at 50 °C and 150 rpm for 72 h with a daily determination

of the released glucose concentration. All of the performed experiments were triplicated and the mean was calculated and listed.

2.4. Enzymatic Degradation

The pretreated samples were washed several times using hot water until neutralization is achieved for use as substrates in the enzymatic degradation. All of the enzymatic hydrolysis treatments are started with 2% of the cellulosic substrate in a total volume of 10 mL acetate buffer (pH 5.5), and are then amended with 100 µL of the cellulase enzyme from *Trichoderma reesei* (≥700 U/g) followed by incubation at 50 °C and 150 rpm for 96 h. During the incubation period, the concentration of released glucose units was determined after 72 h spectrophotometrically using a glucose kit (Biosystem, Barcelona, Spain).

As the amount of the used cellulase enzyme can strongly affect the released glucose units, different amounts of cellulase enzyme were tested against a fixed percentage of the optimum pretreated substrate (CSM) to determine the optimum amount of the enzyme that can produce the highest glucose concentration. From this point of view, 10 tubes of 2% of the pretreated substrate were added to a 5 mL acetate buffer (pH 5.5). The effect of the type of adjusting pH (using acetate buffer or pH adjusted liquids) on the enzymatic degradation has been investigated, as well. Following the incubation of all tubes at 50 °C and 150 rpm for 72 h, the glucose concentration was spectrophotometrically measured every 24 h.

2.5. Yeast Isolation

Isolation of yeast depends on the use of rotten fruit juice as a probable and favorable yeast growing source. From this point of view, fresh apple juice was purchased from local markets and remained open for 1 week at room temperature to allow for the growth and propagation of yeast. In addition, 100 µL of the juice were serially diluted followed by the spreading of 50 µL of each dilution over sterile YPG (yeast extract, 10 g/L, glucose, 10 g/L, peptone, 20 g/L)-containing Petri plates. The plates were incubated at 30 °C for 72 h. Then, the plates were checked for the growth of microbial colonies using a light microscope.

2.6. Molecular Identification of the Yeast Isolate

Following total genomic DNA extraction and PCR amplification of the 18S rRNA gene, 10 µL of the amplified product were checked for the presence of the amplified gene on 1% agarose gel. The obtained data revealed the successful amplification of 1500 pb of the 18S rRNA gene. Then, this PCR amplified product was sent for sequencing to identify the nucleotide sequences of the gene and compare them with the genes deposited in GenBank to determine the genus and species that the isolate belongs to.

2.7. Fermentation Process

In this work, a microbial colony was grown on the surface of the cultivated YPG agar plates. The colony was checked under a light microscope to confirm its identity as a yeast isolate. Following confirmation, the isolated yeast was cultivated in 10 mL YPG broth containing high glucose concentration. Following 72 h of incubation, a sample of the culture was analyzed by HPLC. The isolated yeast colony was individually transferred to YPG broth with elevated concentrations of glucose. The tube was incubated at 30 °C and 150 rpm for 72 h. Following incubation, 1 mL was used for the determination of formed bioethanol using HPLC analysis. To determine the optimum fermentation operating conditions, various parameters have been investigated, such as the aerobic and anaerobic conditions, the fermentation temperature from 25 to 40 °C, the pH of the media from 3 to 11, and the inoculum size from 0.5 to 10%.

2.8. Characterization of CS and CSM

2.8.1. Hemicellulose, Cellulose, and Lignin Contents

Quantitative detection of the CS and CSM hemicellulose, cellulose, and lignin was performed as mentioned by Hamdy et al. [10], where exactly 1 g of the dried sample of CS

and CSM were suspended separately in 70 mL neutral detergent and then autoclaved for 40 min at 100 °C and 20 min at 120 °C. The resulting solid residues were filtered, washed with hot distilled water until pH 6.5–7, washed twice with ethanol, dried overnight at 50 °C, weighed, and labeled as (W_0). Then, the W_0 sample was suspended with 70 mL of 2 mol/l HCl and autoclaved for 60 min at 100 °C. The resulting solid residue was filtered, washed with hot distilled water until pH 6.5–7, washed twice with ethanol, dried overnight at 50 °C, weighed, and labeled as (W_1). The W_1 sample was soaked in 72% H_2SO_4 for 4 h at room temperature, then water was added to the mixture and incubated at room temperature overnight. The resulting solid residue was filtered, washed with hot distilled water until pH 6.5–7, dried overnight at 50 °C, weighed, and labeled as (W_2). Finally, the W_2 sample was burned in a (Barnstead Thermolyne 48000, Ramsey, MN, USA) muffle furnace for 4 h at 575 °C. The resulted powder was weighed and labeled as W_3.

The hemicellulose, cellulose, lignin, and ash contents were estimated using the following equations [10]:

$$\text{Hemicellulose} = W_0 - W_1 \tag{1}$$

$$\text{Cellulose} = W_1 - W_2 \tag{2}$$

$$\text{Lignin} = W_2 - W_3 \tag{3}$$

$$\text{Ash} = W_3 \tag{4}$$

Following the determination of the chemical composition, the % lignin removal, % hemicellulose removal, and % cellulose recovery were calculated according to Equations (5)–(7):

$$\% \text{ lignin removal} = \left(\frac{L_I - (L_F \times \text{ \% Solid recovery yield}/100)}{L_I} \right) \times 100 \tag{5}$$

where % lignin removal is the percentage of lignin removed after the pretreatment process compared with the initial lignin content, L_I is the percentage of initial lignin content, and L_F is the percentage of final lignin content in the solid residue.

$$\% \text{ Hemicellulose removal} = \left(\frac{H_I - (H_F \times \text{ \% Solid recovery yield}/100)}{H_I} \right) \times 100 \tag{6}$$

where % hemicellulose removal is the percentage of hemicellulose removed after the pretreatment process compared with the initial hemicellulose content, H_I is the percentage of initial hemicellulose content, and H_F is the percentage of final hemicellulose content in the solid residue.

$$\% \text{ Cellulose recovery} = \left(\frac{C_F \times \text{ \% Solid recovery yield}/100}{C_I} \right) \times 100 \tag{7}$$

where % cellulose recovery is the percentage of the remaining cellulose after the pretreatment process compared with the initial cellulose content, C_I is the percentage of initial cellulose content, and C_F is the percentage of final cellulose content in the solid residue, where the solid recovery yield was detected according to Equation (8):

$$\% \text{ Solid recovery yield} = \frac{\text{Final pretreated weight (g)}}{\text{Initial CS weight (g)}} \times 100 \tag{8}$$

2.8.2. Proximate Analysis, Ultimate Analysis, and HHV

The proximate analysis was performed to determine the moisture content (MC), volatile matter (VM), fixed carbon (FC), and ash content of the biomass. DIN 51718 standard method was utilized for the determination of the MC by weighing 1 g of CS and CSM on two distinct dried aluminum dishes and heating them in a furnace at 105 °C for 3 h [20]. The MC of CS and CSM was estimated and recorded based on the initial mass of CS and CSM before (M_j) and after the heat treatment (M_f).

DIN 51720 standard method was used to determine the weight reduction (detected from TGA analysis), which is directly proportional to VM and was determined when the weight loss minus moisture at 1 g of sample was heated to 919 °C with a heating rate of 10 °C min^{-1} for 7 min under N_2 atmosphere. On the other hand, DIN 51719 standard method was used to detect the weight of ash by placing it back into the furnace and gradually heating it to 750 °C for 1 h, followed by cooling at ambient temperature in a desiccator.

The ultimate analysis was subjected to determine the CHNS/O elemental analysis of CS and CSM using a Vario-Micro CHN elemental analyzer (Elementar Analyses system GmbH, Langenselbold, Germany). ASTM E-775-78 standard method was utilized to analyze the elements C, H, N, and S during the simultaneous combustion of the gases. Furthermore, by determining the elemental composition, the higher heating value (HHV) can be detected according to the following equation, which is adequate for engineering calculations [21]:

$$\text{HHV} = 0.3419 \times (\%C) + 1.1783 \times (\%H) - 0.1034 \times (\%O) + 0.1005 \times (\%S) - 0.0151 \times (\%N) - 0.0211 \times (\% \text{Ash}) \text{ [MJ/kg]} \tag{9}$$

2.8.3. TGA, FTIR, and SEM Analysis

The thermal stability of CS and CSM samples was explored by thermogravimetric analysis (TGA) using (Shimadzu TGA-50, Kyoto, Japan). The investigation was conducted under a nitrogen atmosphere from room temperature to 919 °C at a heating rate of 10 °C min^{-1}. The heating rate, weight loss, moisture, volatile, ash content, and fixed carbon were recorded for CS and CSM. The FTIR analysis was performed using FTIR (Shimadzu FTIR-8400 S, Kyoto, Japan). The CS and CSM samples were ground with 100 mg KBr to obtain a uniform fine powder. The mixed samples were pressed as pellets using a hydraulic press. The absorption spectra were obtained from 4000 to 500 cm^{-1} with 4 cm^{-1} resolution. A scanning electron microscope was used to obtain the surface morphology images (SEM, JEOL Model JSM 6360 LA, Tokyo, Japan).

2.8.4. Glucose Production Yield

The produced glucose yield was detected spectrophotometrically. Following the enzymatic hydrolysis, 10 mL of the liquid hydrolysate was mixed with 1 mL of glucose buffer (glucose kit, bio-med). This mixture was incubated for 15 min at room temperature. The glucose kit contains glucose oxidase (GOD), which catalyzes the oxidation of glucose to hydrogen peroxide and gluconic acid. Hydrogen peroxide, when combined with 4-amino-antipyrine and a derivative from phenol, forms a red dye compound. The intensity of the produced red color is directly proportional to the glucose quantity in the sample. The red color and consequently the glucose production yield were estimated using a spectrophotometer (7230 G, Shanghai, China) by measuring the absorbance at $\lambda_{\max}$ = 546 nm.

2.8.5. Bioethanol Concentration

The bioethanol concentration was measured using HPLC (Agilent 1100, Santa Clara, CA, USA). The mobile phase was 100% deionized water (DI H_2O), with a flow rate of 0.2 mL/min. The used column was Hi-plex Ca (USP L19) Agilent 250 × 4 mm, 8 μm, and operated at 80 °C. The detector was RI and operated at 55 °C.

2.9. Bioethanol Separation and Purification
2.9.1. Membrane Preparation

Poly (MMA-*co*-MA) membrane was thoroughly dissolved in the respective solvent at 10% concentration polymer (w/w) in DMF. The copolymer was well dissolved in DMF solvent under overnight continuous stirring at ambient temperature and the solution became clear. Then, the homogeneous solution was left for 4 h to release air bubbles.

Thereafter, it was cast on a glass petri-dish with (0.25 mm) thickness. Finally, the prepared membrane was dried at 60 °C in a vacuum for 5 h [22].

2.9.2. Membrane Characterization

The FTIR analysis of poly (MMA-*co*-MA) membranes was performed using FTIR (Shimadzu FTIR-8400 S, Kyoto, Japan). Samples were ground with 100 mg KBr to obtain a uniform fine powder. The mixed samples were pressed as pellets using the hydraulic press. The absorption spectra were obtained from 4000 to 500 cm^{-1} with 4 cm^{-1} resolution.

The surface structure of the synthesized membranes was characterized using SEM (JEOL, JSM-6460LV, Tokyo, Japan) operated at room temperature with an acceleration voltage of 10 kV. The samples were coated with a thin gold-palladium layer prior to measurement using a JFC-1100E sputter (JEOL Ltd., Tokyo, Japan). Thermal degradation and weight loss determination were detected using TGA (Shimadzu TGA-50, Kyoto, Japan). The TGA analysis was performed by raising the temperature from ambient to 800 °C at a heating rate of 10 °C/min in a nitrogen atmosphere.

2.9.3. Water and Ethanol Uptake

Water uptake was detected by immersing the synthesized membranes at room temperature in distilled water for 24 h, drying by wiping with filter paper, and weighing the wet and dry samples. In addition, ethanol uptake was detected by the same procedures as the water uptake, but by immersing the synthesized membranes in pure ethanol rather than distilled water. The water and ethanol uptake is determined by the following equation:

$$W\ (\%) = \frac{W_{wet} - W_{dry}}{W_{dry}} \tag{10}$$

where W_{wet} is the weight of the wet sample (after immersion) and W_{dry} is the weight of the dry sample (before immersion).

3. Results and Discussion

3.1. The Role of Various Organic Acids Pretreatment

Organic acids have the advantages of the selective dissolution of hemicellulose and lignin, protecting and fractionating the cellulose, protecting the environment from pollution, and increasing the equipment's lifetime by avoiding the equipment corrosion that can occur from the use of mineral acids, such as H_2SO_4 [23]. The efficiency of various organic acids, such as maleic acid, oxalic acid, succinic acid, and lactic acid toward the CS pretreatment is evaluated by comparing the compositions of the raw CS with the resulting residues after the chemical pretreatment, as presented in Figure 2. Moreover, the effect of the pretreatment on solid recovery, hemicellulose removal, cellulose recovery, and lignin removal is summarized in Table 1. The interaction between the different organic acids pretreatments and their reflection on the enzymatic degradation is represented in Figure 3. By comparing the four different carboxylic acids, the results evidenced that maleic acid provides the highest cellulose recovery (≈98%) and the highest hemicellulose and lignin removal (≈45% and 53%), respectively. Consequently, it produced the highest glucose concentration of 741.4 mg/dL. This may be related to the fact that maleic acid has a combination between the effect of two carboxylic groups and a conjugated system, which can increase its acidic strength and lead to efficient hemicellulose and lignin hydrolyzing, while oxalic acid, succinic acid, and lactic acid have hydroxyl groups, which lead to a decrease in their acidic strength.
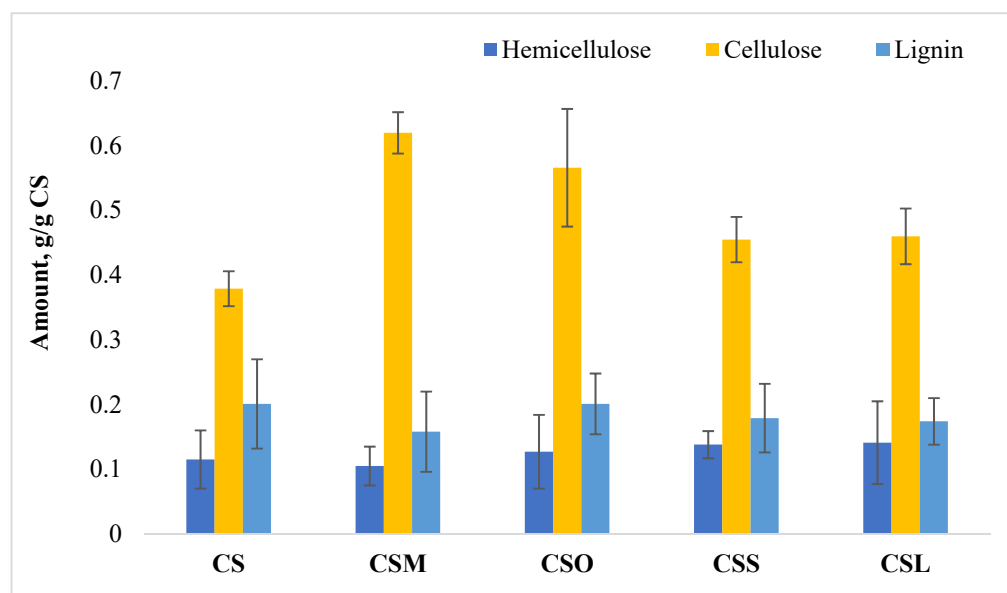
Figure 2. Composition of untreated and treated CS with various organic acid pretreatments. The values are based on the total weight of untreated CS using a pretreatment condition of 2% organic acids, 120 °C under 45 psi at autoclave for 1 h of residence time.

Table 1. Composition of raw and pretreated biomass.

Sample Code	Solid Recovery, %	Hemicellulose Removal, %	Cellulose Recovery, %	Lignin Removal, %
CS	-	-	-	-
CSM	60	45.22	98.15	52.84
CSO	60	33.74	89.6	40
CSS	83	0.04	99.64	26.08
CSL	81.5	0.07	98.92	17.49

According to the literature [24], the efficiency of the pretreatment increases with the lower pH value. Therefore, maleic acid has a higher acid strength than oxalic, succinic, and lactic acid and thus, the maleic acid pretreatment is the most effective for delignification and enzymatic cellulose digestibility to glucose monomers, as shown in Figure 3. Moreover, maleic acid is the most favorable for hemicellulose dissolution, which can be clarified by the dicarboxylic structure of maleic acid that does not entirely release hydrogen ions in an aqueous solution [23]. Under acidic conditions, hydrogen ions attack the ether or ester bonds between hemicellulose and lignin, which are prone to dissociate, while the unreleased parts interact directly with –OH groups on the rings of hemicelluloses that lead to being effectively dissolved into the pretreatment with maleic acid. Furthermore, oxalic acid has a high glucose yield of 670 mg/dL as a result of high cellulose recovery (89.6%), in addition to the high hemicellulose and lignin removal (33.7 and 40%), respectively. Although the CS pretreated samples using succinic and lactic acids have the highest cellulose recovery, they released the lowest glucose concentration after the enzymatic degradation. This may be due to the succinic and lactic acids pretreatments, which are inefficient in hemicellulose removal, did not exceed 1%, and are due to their tenuous effect on the lignin removal. This may complicate the cellulase enzyme accessibility to the recovered cellulose to convert it to glucose. Therefore, the results proved that the combination of the high cellulose recovery with the hemicellulose and lignin removal enhances the enzymatic degradation and motivates the glucose concentration, not only for one of them. The aforementioned results revealed that maleic acid can be considered the optimum carboxylic acid that can be utilized in the further production stages. Furthermore, it was concluded that 72 h of

incubation time would be sufficient for the enzymatic degradation process completion and could be subjected to the following stages of the bioethanol production process.
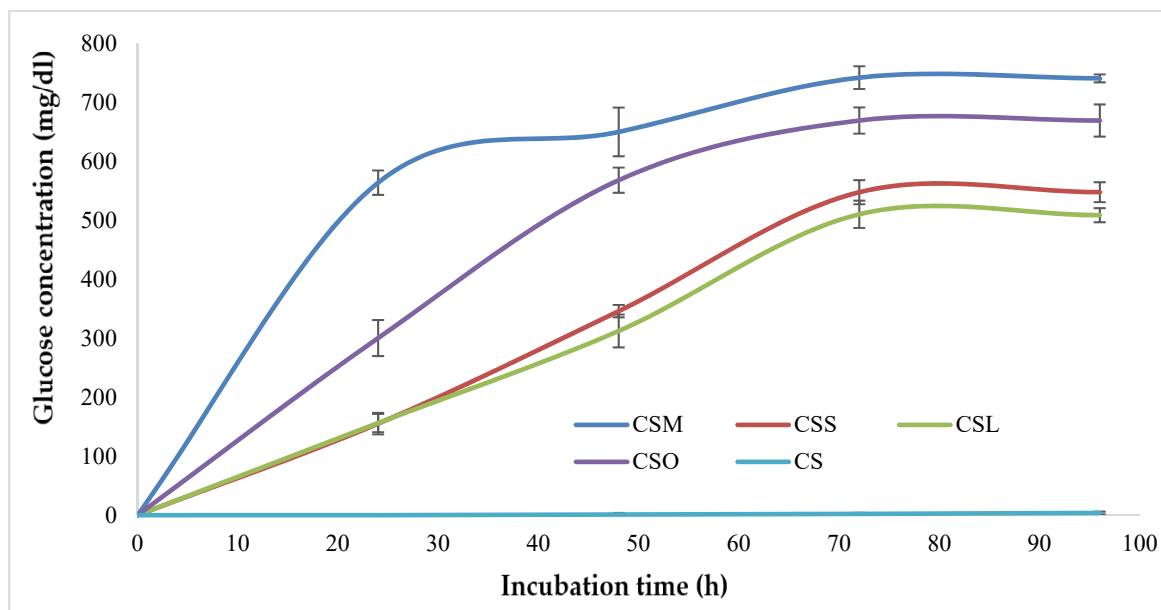

Figure 3. The glucose concentration after various organic acid pretreatments and enzymatic treatments of the solid cellulosic matrices during the incubation period. The enzymatic operating condition: 2% cellulosic matrices in 10 mL acetate buffer (pH 5.5), 100 μL cellulase enzyme (≥700 U/g), incubated at 50 °C and 150 rpm for 96 h.

3.2. Proximate Analysis

The proximate analysis results of CS and CSM are shown in Table 2. The percentage content of MC, VM, FC, and ash derived from CS and CSM were within the literature range in terms of proximate composition [25]. The analysis of the data reveals that CSM has a lower MC than CS. The large content of VM of CS (70.63%) represents a high yield of production of fuel. The VM content of CS is higher than the other biomass fuels, for example, oil palm fiber (65.75 wt%) [26], rice husk (65.33 wt%) [27], and *Mbwazirume* peel (MP) and *Nakyinyika* peel (NP) (69.99 and 19.98 wt%), respectively [25]. Interestingly, it reveals that CSM has a high VM than CS, indicating that the pretreatment of CS by maleic acid leads to boosting fuel production. Furthermore, the higher the fuel volatile concentration, the higher the HHV, and the less heat required for thermochemical reactions.
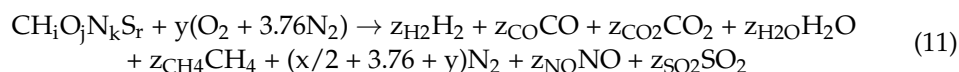
Table 2. The proximate and ultimate composition of CS and CSM.

Samples	Proximate Analysis				Ultimate Analysis					HHV (MJ·kg^{-1})
	MC	VM	Ash	FC	C	H	N	O	S	
	(wt%)				(wt%)					
CS	10.09	70.63	2.2	17.08	35.36	5.32	0.26	58.44	0.62	13.11
CSM	8.05	83.63	2.0	6.32	37.42	5.39	0.26	56.86	0.07	13.38

As known, in fuel production, ash is an unwanted component. The ash content of the samples reveals an intriguing phenomenon in this context. The low percentage of ash content, as observed in Table 2, confirmed that this pretreatment is promising for the production of clean fuel due to its low ash content. The FC is the amount of ash-free carbon that remains after the VM. The percentage of FC in CS was reduced after the pretreatment using maleic acid from 17.08 wt% in the CS sample to 6.32 wt% in the CSM sample.

3.3. Ultimate Analysis and HHV

The ultimate analysis of biomass fuels was achieved in this study using simultaneous combustion, in which (C, H, O, N, and S) react with the exothermic reaction process and produce CO_2, H_2O, NO_x, and SO_2, respectively [25]. Equation (11) represents the degradation of biomass fuels, as follows [25]:

$$CH_iO_jN_kS_r + y(O_2 + 3.76N_2) \rightarrow z_{H2}H_2 + z_{CO}CO + z_{CO2}CO_2 + z_{H2O}H_2O \\ + z_{CH4}CH_4 + (x/2 + 3.76 + y)N_2 + z_{NO}NO + z_{SO2}SO_2 \tag{11}$$

As shown in Table 2, the ultimate composition of CS and CSM observed in this investigation differs slightly. C, H, and O contents are quite high in MP, while N and S concentrations are low. According to the literature, the drop in H and O concentrations in CS and CSM has been linked with the scission of weak bonds within the char structure [28]. Furthermore, CS had low S and ash contents, indicating that it has suitable prospects for biofuel generation when compared with coal, which has a S and ash level of 0.5 and 7.5% [21], and other biomass wastes presented by other studies [25,29]. Following the pretreatment using maleic acid, the S and ash contents are decreased, which indicate that CSM has higher production of biofuel when compared with CS. Furthermore, since the S and N contents are very low, it is claimed that no processing or technology is required to reduce the exhaust emission of sulfur oxides (SO_x) and nitrogen oxides (NO_x) from this biomass waste. In addition, the carbon content in CSM is higher than CS, which may be related to the generation of new hydroxyl groups as well as hydrolysis of methoxy groups and ether bonds [12]. C and O are proportional to the HHV or calorific value of the fuel, which indicates whether the biomass is suitable for use as a fuel or not. The calorific values of CS and CSM were 13.11 and 13.38 MJ·kg^{-1}, respectively which may be significant for biofuels production. From these investigations, CS qualifications for biofuel production have been improved after the pretreatment using maleic acid.

3.4. Thermal Analysis

The TGA curve of CS and CSM was determined in Figure 4. At temperatures up to 919 °C, three distinct zones are identified, which are associated with the elimination of cellulose, hemicellulose, and ultimately lignin, according to the thermal results obtained. Drying (water removal), devolatilization (release of organic matter), and slow combustion (oxidation of bonded carbon) are three stages in weight loss during the thermal degradation of CS and CSM. Furthermore, the pyrolysis decomposition of CS and CSM in the nitrogen atmosphere is classified into hemicellulose (100–250 °C), cellulose (300–500 °C), and lignin (500–650 °C), taking into account that there is little weight loss below 100 °C as a result of the existence of humidity. Figure 4 shows that temperatures reaching upwards of 370 °C (for CS) and 388 °C (for CSM) led to a meaningful weight reduction due to pyrolysis of the biomass [12]. The decomposition of CS at (>670 °C) and CSM at (>634 °C) was observed as a result of the breaking of the bonds of the lignin. Overall, the CSM has more thermal stability and higher char yield (19.28%) than CS (8.32%).

3.5. Functional Analysis

To explore the functional groups attached to the CSM and their changes, the FTIR spectra were performed in the range of 4000–400 cm^{-1} (Figure 5). The band around 3340 cm^{-1} is due to the OH stretching vibrations that indicate the presence of alcohols, syringyl groups of lignin, hydroxyphenyl, chemisorbed water, and phenols that are present on cellulose and lignin in CS and CSM [10,30]. The band at 2909 cm^{-1} in the case of the CSM sample is lower than the intensity in the case of the CS sample. This band corresponds to aliphatic structures of asymmetrical C–H stretching vibrations of lignin and/or hemicelluloses [6,31]. The lower peak intensity in the case of CSM indicates lignin and/or hemicelluloses reduction than the intensity presented in the CS sample. Following the pretreatment process, the intensity of the band at 1628 cm^{-1}, which is corresponding to

the C=O to C–OH group transformation, is decreased and reflected the lignin reduction [32]. The band at 1232 cm^{-1} in the CS sample is corresponding to guaiacyl/syringyl ring and C–O stretching vibration, which is related to the production of guaiacol and/or glyoxal, in addition to the presence of syringyl and guaiacyl in the remaining lignin and/or xylan. Following the pretreatment process, this band is shifted to 1230 cm^{-1} and its intensity is decreased, which indicates that C=O resulted from the cleavage of acetyl groups and lignin reduction, respectively [33]. The very sharp bands at 1031 cm^{-1} that are observed in the two samples with high intensities are attributed to C–OH bending in β-(1,4)-glycosidic linkages between glucose and cellulose, C–C stretching, C$_1$–H deformation with ring vibration, and C–O–C, which are cellulose characteristic bands for pyranose ring skeletal vibration [6]. Two bands at 554 and 455 cm^{-1}, which existed in the CSM sample and not in the CS sample and are related to C–OH bending, are the main characteristics of cellulose. The aforementioned analysis proved the successful cellulose fractionation and successful delignification process, as well.
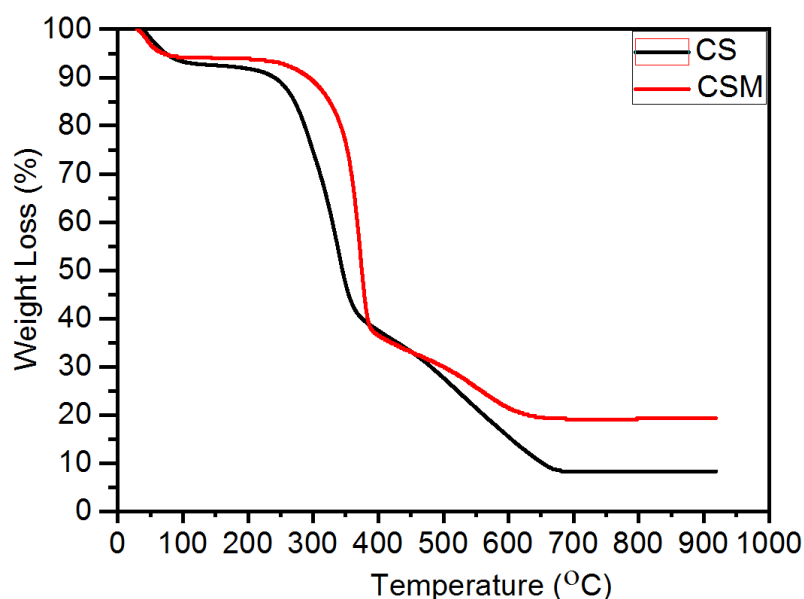

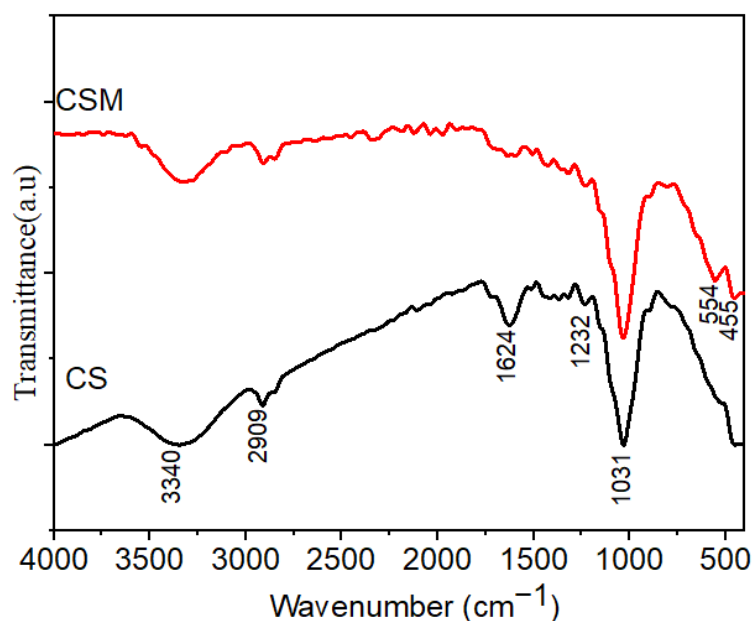**Figure 4.** TGA curve of CS and CSM.

Figure 5. FTIR spectra of CS and CSM.

3.6. Morphological Characteristics

The impact of the pretreatment with maleic acid on the complex structure of CS is shown in Figure 6. The surface morphology of the CS sample, which was detected at a magnification of 200 and 1000×, exhibited a compact high fiber content and demonstrated the existence of high cellulose content (as described in Section 3.1). As shown in Figure 6a,b, the CS sample is highly ordered with a low degree of porosity. Following the maleic acid pretreatment, it exhibited an irregular morphology with cavities and cracks due to the successful removal of lignin and hemicellulose from CS. This may be a useful result in bioethanol production.

Figure 6. SEM images of (**a**,**b**) CS and (**c**,**d**) CSM.

3.7. The Role of Maleic Acid in the Delignification Process

This study proposed a suitable mechanism for lignin dissolution by maleic acid (Figure 7). Lignin structure (1) which has β-O-4 aryl ether linkage (with red color) (2) can be oxidized to give β-O-4 phenoxy acetophenone (3). The oxidation of β-O-4 aryl ether linkage decreases the enthalpy dissociation of the C–O aryl ether bond, which allows more mild cleavage conditions to be employed. The lone pair of oxygen in compound (2) will attach the hydrogen ions (H$^+$) that are present in the solution to give an unstable intermediate, which reacts with hydrogen oxalate to give the compound (4). Then, compound (4) reacts with molecular oxygen for the production of an unstable intermediate dioxetane (5), which may react with two pathways. First, pathway A, a ring of dioxetane (5) is opened to give hydroperoxide (6), which can be reduced to give alcohol (7). The acid-mediated solution leads to guaiacyl/syringyl ring and C–O bond cleavage as detected by FTIR analysis (the peak at 1235 cm^{-1} which is shifted to 1230 cm^{-1}) to give two products: Guaiacol (8) and glyoxal (9). Glyoxal can attach to water and convert formic acid into anisaldehyde (12) through 1,2-hydride shift giving (11), which produces formic acid as a by-product through rearrangement to give the compound (12) that gives p-anisic acid (13) by oxidation. Second, pathway B, dioxetane (5) undergoes ring-opening by C–C bond cleavage to give p-anisic acid (13) and phenyl formate (14). The acidic reaction conditions form phenyl formate (14)

that undergoes cleavage easily to give guaiacol (8) [34,35]. One of the end products from pathways A and B is guaiacol, which is soluble in water and leads to lignin dissolution.
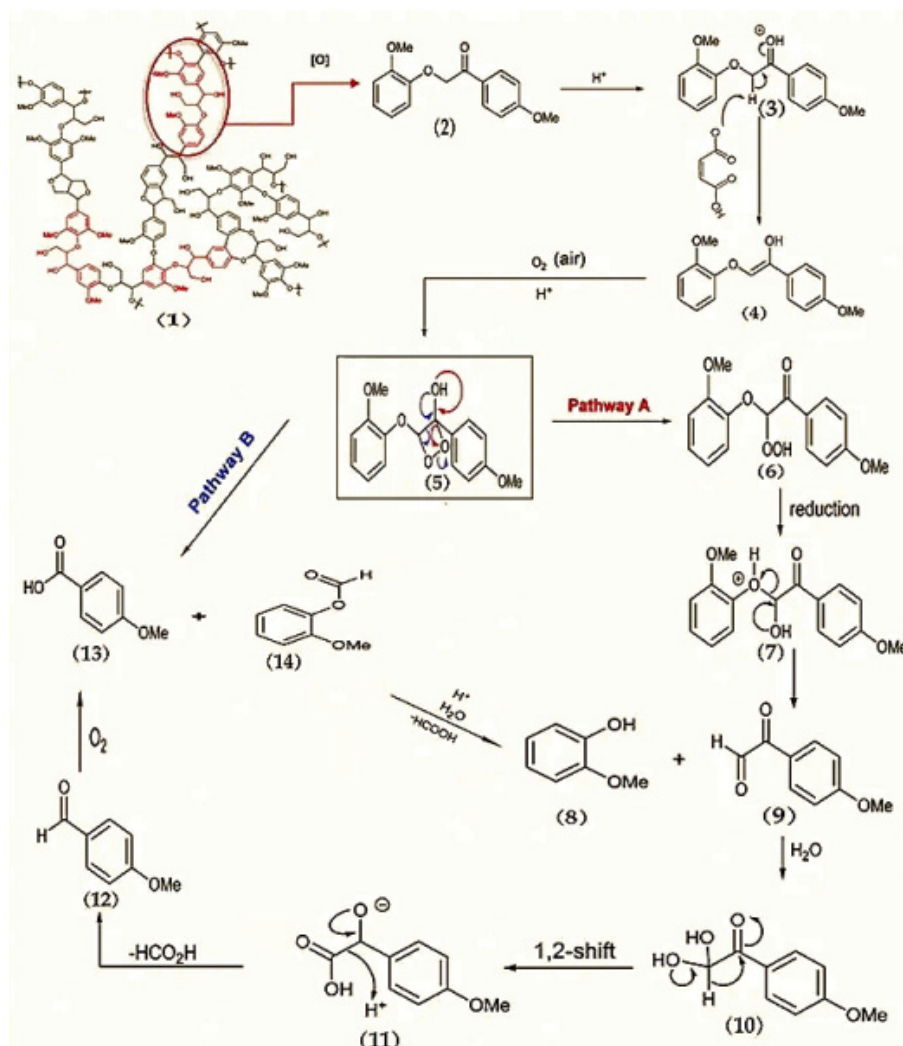

Figure 7. Proposed mechanism of CS delignification using maleic acid.

3.8. Optimization of the Pretreatment Process

The pretreatment process has been optimized by investigating the impacts of various conditions (i.e., maleic acid concentration, incubation time, solid-to-liquid ratio, and temperature) on the released glucose concentration after the pretreatment process. Figure 8a shows that as the maleic acid concentration increased in the pretreatment process from 1 to 2% the glucose concentration is significantly increased from 702 to 741 mg/dL. The glucose concentrations released from the enzymatic hydrolysis of the CS pretreated samples using maleic acid with higher concentrations (3–7%) are close. These results suggest that the oxidation of lignin and its delignification and the hemicellulose removal reached 53 and 45%, respectively by maleic acid (Table 1). In addition, this may reach about the maximum using 2% maleic acid, and the remaining linkages in the lignin and hemicellulose were nearly stable and not affected by the increase in the maleic acid concentration. Therefore, from an economical point of view, 2% maleic acid could be recorded as the optimum maleic acid concentration of the pretreatment process. As shown in Figure 8b, the amount of the produced glucose units was time-dependent. The glucose concentration was proportional to the applied autoclaving time at lower periods (10 and 60 min). At these times, the glucose concentration was increased from 451 to 741 mg/dL, respectively. On the other hand, the elevated autoclaving times (90 and 120 min) resulted in decreasing the glucose

concentration to reach 594.498 and 528.155 mg/dL, respectively. Therefore, the autoclaving time of 60 min was recorded as the optimum time that resulted in the highest release of glucose units. These results are matched with Banoth et al. [36] who reported that the pretreatment of rice straw with steam and pressure (autoclaving) at 120 °C for 60 min decreased the hemicellulose by 60.8% hemicellulose recovery and accordingly produced the highest fermented sugars yield. Moreover, Lyu et al. [21] reported compatible results, which revealed that by exceeding the autoclaving time of 60 min the cellulose recovery is reduced sharply, which may be due to carbohydrate decomposition after a certain delignification level that led to the direct exposure of cellulose to the acid [37]. The opened path between the carbohydrate constituents of cellulose and the maleic acid led to attacking and decomposing the carbohydrate and consequently reduced the released glucose concentration. The effect of the solid-to-liquid ratio during the pretreatment process on the enzymatic degradation is shown in Figure 8c. Decreasing the solid-to-liquid ratio from 1:10 to 1:20 in the pretreatment process increases the glucose concentration from 681 to 741 mg/dL. These results revealed that the CS to maleic acid ratio of 1:10 represents an insufficient acidic medium to diffuse the solid substrate efficiently and dissolute the lignin successfully, which leads to low glucose yield. The use of a lower CS to the maleic acid ratio of 1:20 released higher glucose concentration. This may be attributed to the efficient interaction between the CS substrate and the maleic acid where the CS substrate ratio was decreased, which increased the contact with the acid medium and increased the lignin and hemicellulose dissolution. Further decrease in the CS ratio than 1:20 to reach 1:50 decreases the released glucose from 741 to 658 mg/dL, which may be a result of excessive lignin and hemicellulose dissolution and cellulose breakdown, as well. Therefore, these results proved that 1:20 CS to maleic acid provides an adequate acid medium that is necessary to dissolve lignin and hemicellulose, protect the cellulose content from breakdown and decomposition, fractionate the cellulose efficiently, and could be considered as the optimum solid-to-liquid ratio. Figure 8d shows that the use of the autoclaving temperature of 90 °C releases the lowest glucose concentration, which indicates that this temperature may be insufficient to dissolve the lignin successfully. The glucose concentration, which is released after the pretreatment using the autoclaving temperature of 100 and 110 °C, is very close. However, the CS pretreatment using the autoclaving temperature of 120 °C leads to the production of the highest glucose concentration, which may be related to the high lignin and hemicellulose removal (53 and 45%), respectively and the high cellulose recovery (98%), as mentioned in Table 1. It is considered that the increased temperature accelerated the release of hydroxonium ions ($^+$OH) from maleic acid to provide a robust electrophilic agent that can react with lignin for ring hydroxylation, oxidative ring-opening, epoxidation, and cleavage of β-aryl ether bonds, resulting in the facilitating dissolution of lignin [38].

3.9. Molecular Identification of the Yeast Isolate

Following DNA extraction and PCR amplification of the 18S rRNA gene, the PCR amplified product was sent for sequencing to identify the nucleotide sequences of the gene and compare them with the genes deposited in GenBank to determine the genus and species that the isolate belongs to. The obtained data revealed that the isolated yeast strain is close to *Pichia nakasei* with a similarity of 98%. Then, the sequence was deposited in GenBank with the accession number MZ675535.

3.10. Optimization of Fermentation Parameters

The total volume of acetate buffer that contains the liberated glucose units after enzymatic hydrolysis was distributed into small volumes that were subsequently submitted for the fermentation parameters. It is worth mentioning that the final measured glucose concentration that was considered as the initial glucose concentration for all fermentation parameters was about 741 mg/dL.
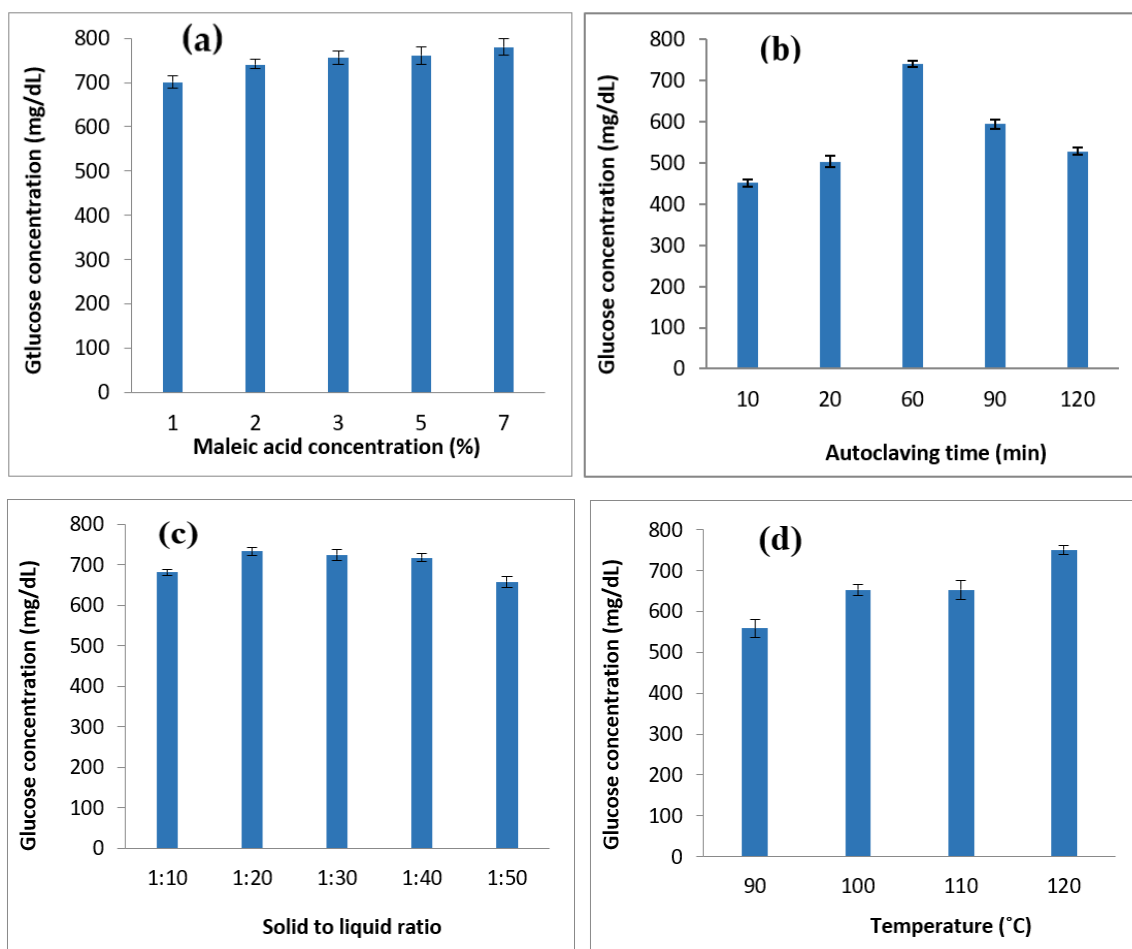
Figure 8. Glucose concentration release using different pretreatment processes. (**a**) Effect of maleic acid concentration; (**b**) effect of autoclaving time; (**c**) effect of solid-to-liquid ratio; (**d**) effect of temperature (2% maleic acid, 120 °C for 60 min, 1:20 solid-to-liquid ratio).

3.10.1. Incubation under Aerobic and Anaerobic Conditions

The ability of the yeast isolate to ferment the sugar into bioethanol at various aerobic and anaerobic conditions is evaluated. The tested yeast isolates succeeded in fermenting the glucose units into bioethanol. It has been observed that the incubation under anaerobic conditions was favored for the yeast isolate and showed higher bioethanol production yield (390 mg/dL) for 72 h compared with 278.6 mg/dL under aerobic conditions for the same time. These results revealed that the anaerobic conditions are more favorable than the aerobic conditions regarding bioethanol synthesis by the yeast strain. In most of the previously reported cases, the yeasts always preferred the anaerobic conditions for the bioethanol production than the aerobic conditions which agree with these results [39].

3.10.2. Incubation Temperature

The influence of temperature on the fermentation process is important for the determination of the ideal temperature, which is consistent with the yeast and the other parameters that contribute to the maximum bioethanol production. Figure 9a shows the bioethanol concentration by the yeast isolate under different incubation temperatures. The results show that 30 °C is the most favorable incubation temperature for the yeast isolate. The isolate recorded a bioethanol concentration of 537.42 and 532.34 mg/dL at 30 and 35 °C, respectively. Therefore, it can be concluded that 30 °C is the optimum incubation temperature of the fermentation process that leads to maximum bioethanol concentrations.

At higher incubation temperature, the bioethanol production yield decreased which agrees with the results reported by Periyasamy et al. [40].
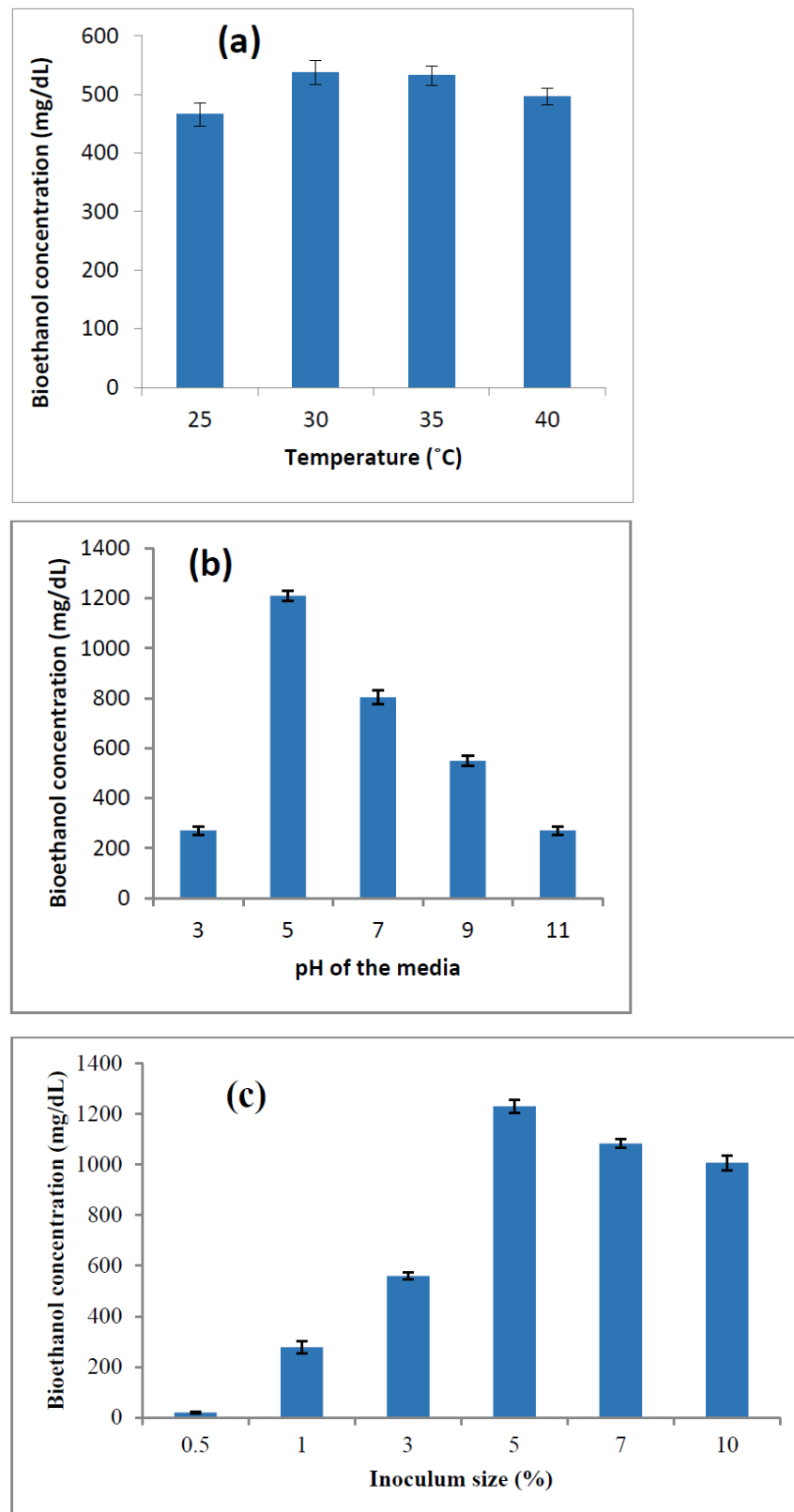

Figure 9. Effect of (**a**) incubation temperature, (**b**) pH of the media, and (**c**) inoculum size on the bioethanol concentration using the isolated yeast strains.

3.10.3. pH of the Media

The effect of pH on the bioethanol concentration using the yeast isolate has been investigated using a pH range from 3 to 11, as shown in Figure 9b. It has been detected that lower pH values resulted in a lower bioethanol concentration compared with neutral or slightly acidic or alkaline conditions. At pH 3 and 11, the bioethanol concentration was in its lower value of 270.9617 mg/dL for both pH values. The concentration of bioethanol was gradually decreased from 803.8787 to 550.1087 mg/dL when the pH changed from 7 to 9, respectively. However, the maximum bioethanol concentration of 1209.9 mg/dL was recorded at pH 5. The results show that the pH is an important factor that positively affects the yeast growth and fermentation rate. However, the optimum pH value is largely dependent on the type of cultivating organism [41]. Therefore, these results indicate that the isolated yeast strain is able to produce a high bioethanol concentration, and pH 5 is the most favored among the other tested pH values.

3.10.4. Inoculum Size

The number of microbial cells that are able to ferment the glucose units into bioethanol is an important factor that should be optimized. Different inoculum sizes of the yeast isolate have been tested for their bioethanol production capability. As shown in Figure 9c, the lower inoculum size of the isolate resulted in a lower bioethanol concentration. The use of 0.5% inoculum size resulted in almost no ethanol production even after 72 h of incubation. The gradual increase in the inoculum size to 1% resulted in the production of bioethanol concentrations of 278.6 mg/dL. These concentrations were elevated to 560 mg/dL using a 3% inoculum size of yeast isolate. On the other hand, it has been observed that the maximum bioethanol production yield was monitored as 1230 mg/dL using the 5% inoculum size of the yeast isolate. Increasing the inoculum size to 7 and 10% decreased the bioethanol concentration to 1083 and 1006.9 mg/dL. Therefore, it could be concluded that the 5% inoculum size is optimum for the highest bioethanol concentration. These data revealed that using inoculum sizes that are higher or lower than the optimum resulted in a fermentation yield reduction.

3.11. Bioethanol Separation and Purification

3.11.1. Physico-Chemical Characterization of Polymer Membranes

Figure 10a shows the FTIR spectra of poly (MMA-*co*-MA) membrane. The band at 3532 cm^{-1} is due to the stretching vibration of –OH [10]. The asymmetric and symmetric stretching vibration band of CH$_2$ and/or CH$_3$, which is the main characteristic for functional groups of PMMA and PMA, was detected at about 2954 cm^{-1} [42,43]. The stretching of the C=O ester group is attributed to the band at 1744.68 cm^{-1}, which is considered as another characteristic for the function groups of PMMA and PMA that compose the poly (MMA-*co*-MA) membrane [44,45]. The peak at 1440 cm^{-1} attributed to O–CH$_3$ bending. The split bands at 1260 and 1215 cm^{-1} represent the C–O stretching [46]. The peak at 834 and 703 cm^{-1} is ascribed to CH$_2$ asymmetric and symmetric rocking, respectively [47]. At 1084 cm^{-1}, there is a medium-sized absorption band of bending vibrations coupled with the rocking vibrations of CH$_3$–O and CH$_3$. Stretching vibrations of C–C–O (skeletal) coupled with stretching vibrations of C–O result in a split band at 1260 and 1215 cm^{-1}, respectively. From these observations, it is clear that co-polymerization was performed successfully between PMMA and PMA [48].

SEM examination has also been subjected to explore the morphology of the synthesized poly (MMA-*co*-MA) membrane, as shown in Figure 10b. SEM was used to observe the top surface and cross-sectional morphological features of the flat-sheet membranes using several magnification scales. An SEM image reveals no phase separation or membrane damage, suggesting that the membranes are suitable for the bioethanol separation process. In addition, SEM images of poly (MMA-*co*-MA) membrane show a rough and irregular surface. Some voids are observed at the membrane surface demonstrating a successful co-polymerization process.
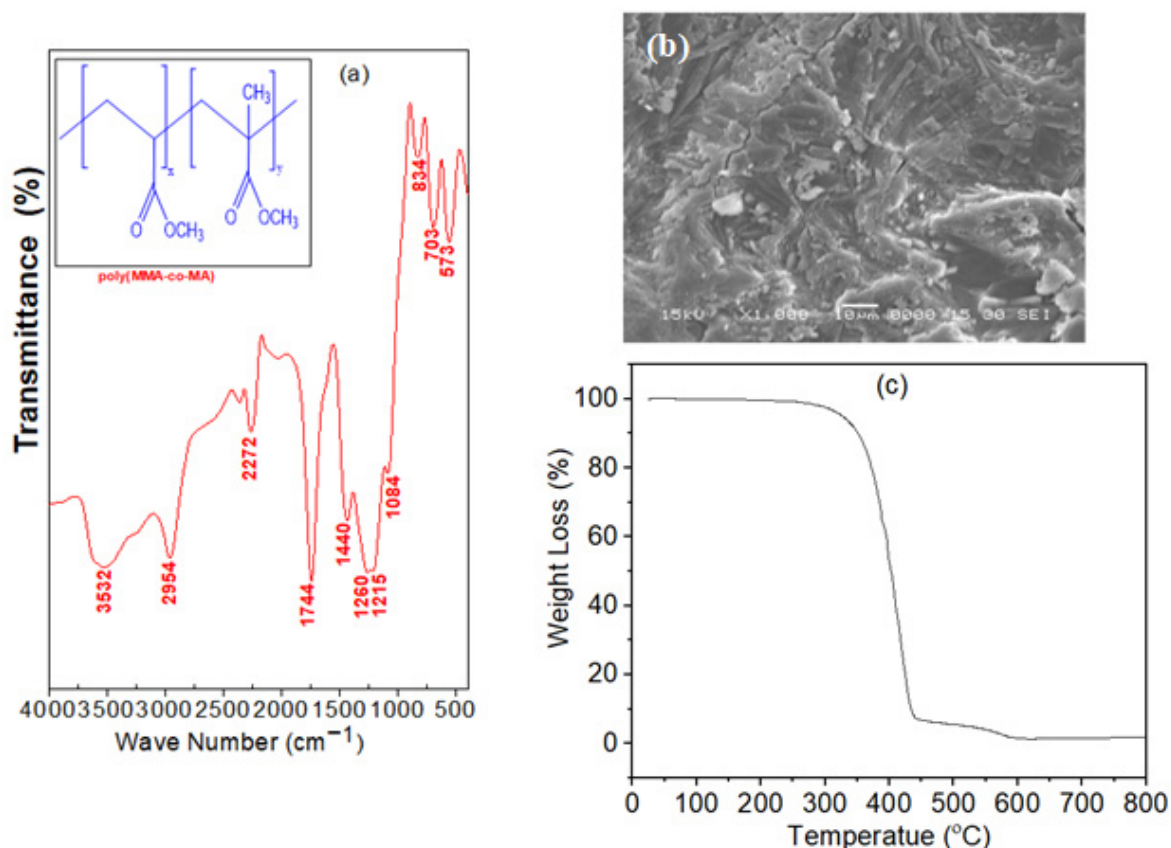
Figure 10. (**a**) FTIR spectra, (**b**) SEM, and (**c**) TGA of poly (MMA-*co*-MA) membrane.

The thermal stability of poly (MMA-*co*-MA) membrane in Figure 10c showed only 1.3% weight loss at the temperature range from 267 to 800 °C and a total weight loss of 94% from the total mass owing to a slight degradation of the PMA chain. Additionally, this is due to a mechanism that involves random hemolytic backbone bond scission as an initiator. These results illustrated that the copolymer has high thermal stability at a temperature lower than 300 °C as a result of the existing MMA and MA, which enhance the thermal stability of the copolymer [49].

3.11.2. Water and Ethanol Uptake

The water and ethanol uptake is correlated with the capability of polymer membrane to permeate and absorb water if it has a hydrophilic feature or ethanol if it has a hydrophobic feature after immersing a piece of polymer membrane in ethanol and water for 24 h separately. The water and ethanol uptake for poly (MMA-*co*-MA) membrane showed that the prepared film was water-insoluble and can absorb only 30% water and the ethanol uptake was 68%.

3.11.3. Application of the Polymeric Membrane in Ethanol Separation

The separation of ethanol from water was deliberated in a few studies which elaborated on many separation techniques. Nowadays, the pervaporation technique has become the preferred technique for separation technology [50]. The current work depends on the same mechanism of pervaporation using poly (MMA-*co*-MA) membranes. The separation process was accomplished on an ethanol/water source with a concentration of 25% ethanol in water. Moreover, the bioethanol purification after the fermentation process was applied for the separation process. Various nitrogen pressures were applied for several hours as shown in Figure 11 (and mentioned in Supplementary Materials Tables S1–S4). It was observed that the highest permeate volume and the highest permeate concentration were monitored at a significantly low pressure of 30 psi.
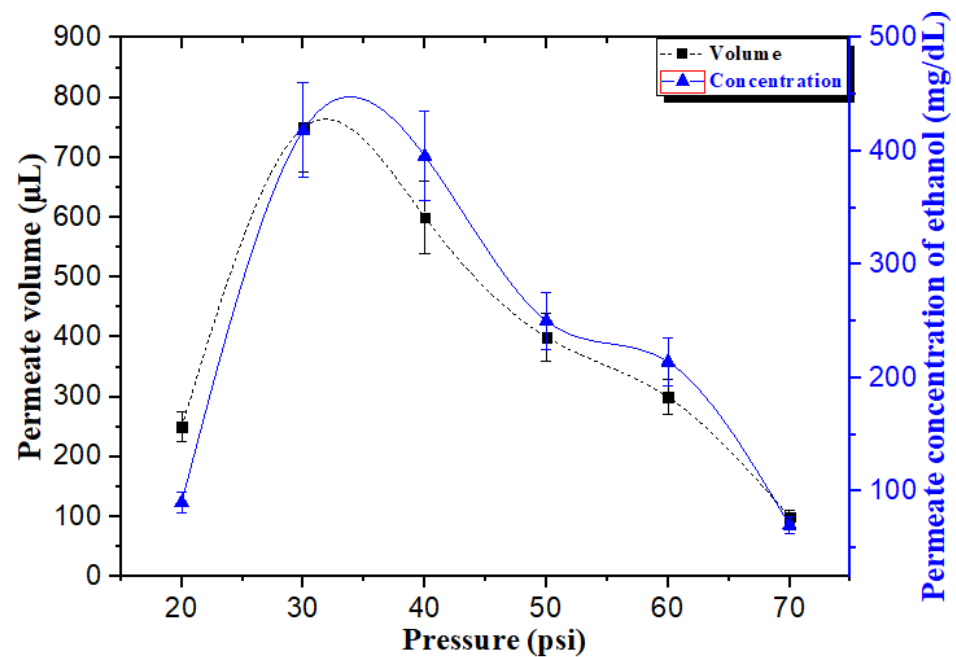
Figure 11. Pervaporation process of 25% ethanol to water using poly (MMA-*co*-MA) membrane under different nitrogen pressures.

Figure 12 exhibited that the flux of permeate was 610.282 (mg/m^2·h) at a nitrogen pressure of 30 psi, which resulted from the use of poly (MMA-*co*-MA) membrane and led to the highest separation factor of 77.26 at a nitrogen pressure value of 70 psi.
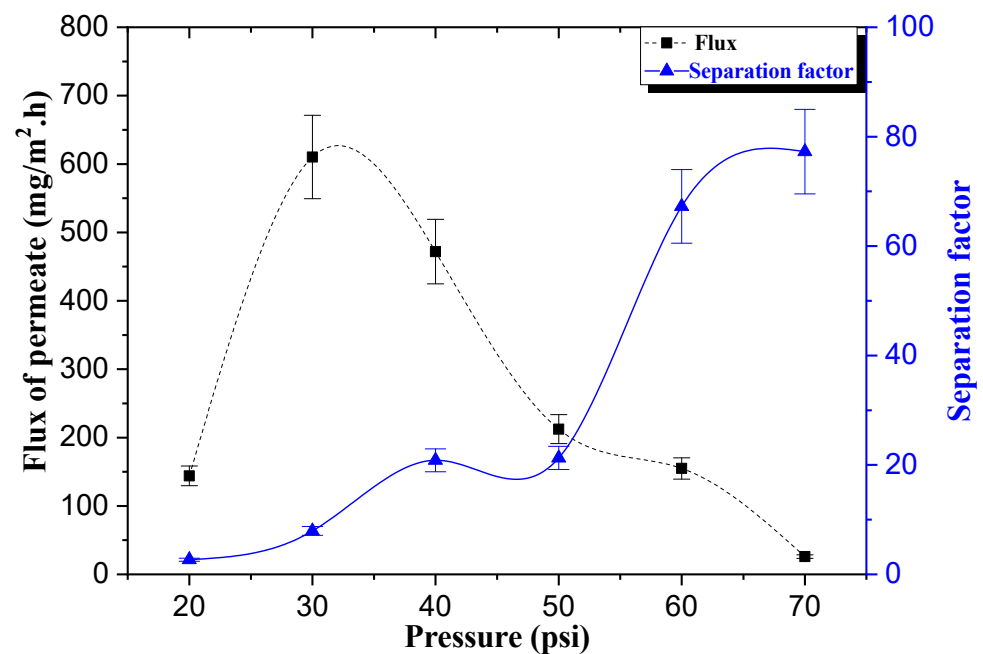

Figure 12. The flux of permeate and separation factor of pervaporation process at 25% ethanol from water using poly (MMA-*co*-MA) membrane under different nitrogen pressures.

On the other hand, the produced bioethanol from the fermentation process (as mentioned in Supplementary Materials Tables S3 and S4) represents the separation process via poly (MMA-*co*-MA) membranes and proves that the highest permeate volume was recorded at a nitrogen pressure of 30 psi, as shown in Figure 13.
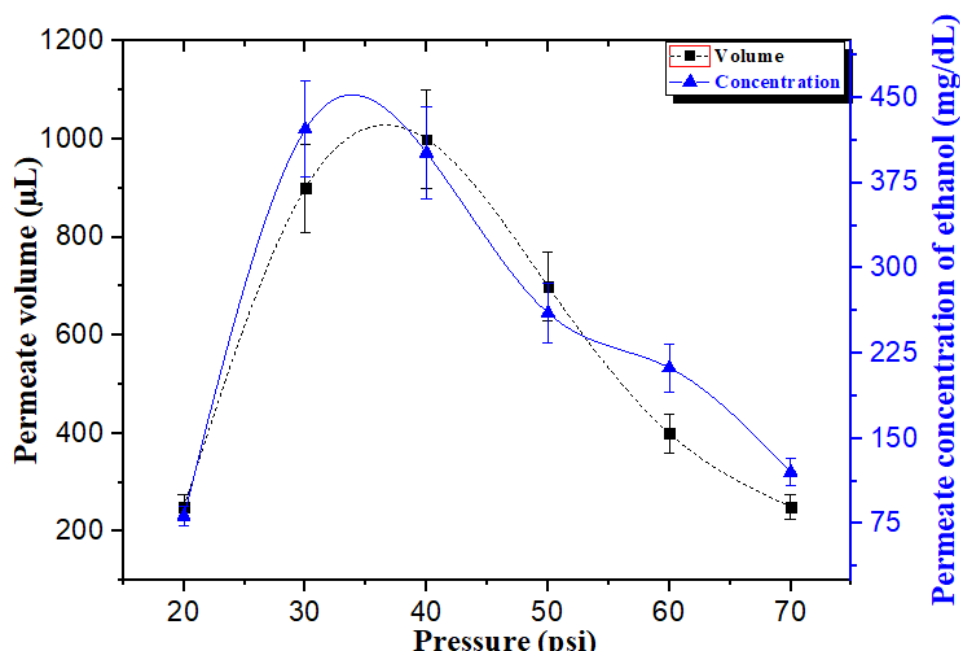
Figure 13. Separation process of fermentation broth using poly (MMA-*co*-MA) membrane under different nitrogen pressures.

The use of poly (MMA-*co*-MA) membrane increased the permeate volume from 250 to 1000 μL, the highest permeate volume, by raising the nitrogen pressure from 20 to 30 psi and then decreasing it. Figure 14 revealed that the highest flux of permeate using poly (MMA-*co*-MA) membrane was 618.52 (mg/m^2·h) at a nitrogen pressure of 30 psi and the highest separation factor was 75.13 at a nitrogen pressure of 70 psi. It is worth mentioning that the flux of permeate, separation factor, and ethanol concentration were calculated according to Abu-Saied et al. [51]:

$$\text{Separation factor } (\beta_i) = \frac{Y_i/(1 - Y_i)}{X_i/(1 - X_i)} \tag{12}$$

where X_i and Y_i are the mass fractions of the components on the feed and permeate side, respectively.

These results illustrate that the poly (MMA-*co*-MA) membrane increased the ethanol and bioethanol concentrations efficiently. Poly (MMA-*co*-MA) membrane led to raising the ethanol concentration from 25 to 75.68% and increased the bioethanol concentration in the fermentation broth from 30 to 76.33%. Therefore, the obtained results confirm that the synthesized membrane has an hydrophobic characteristic and is effective for ethanol separation from water and fermentation broth.

3.12. Techno-Economic Study of Bioethanol Production from Corn Stover

The economic study is an assessment of the practicality of a proposed plan or project. It is also an analysis that considers all of a project's relevant factors—including economic, technical, legal, and scheduling considerations—to ascertain the likelihood of completing the project successfully. Therefore, the economy is consistent with the technical or operation conditions.

The bioethanol plant would be designed with a capacity of 32 thousand tons per year (KTA) in 330 working days. The lifetime of the plant is estimated to be 25 years beginning from 2023 to 2047.
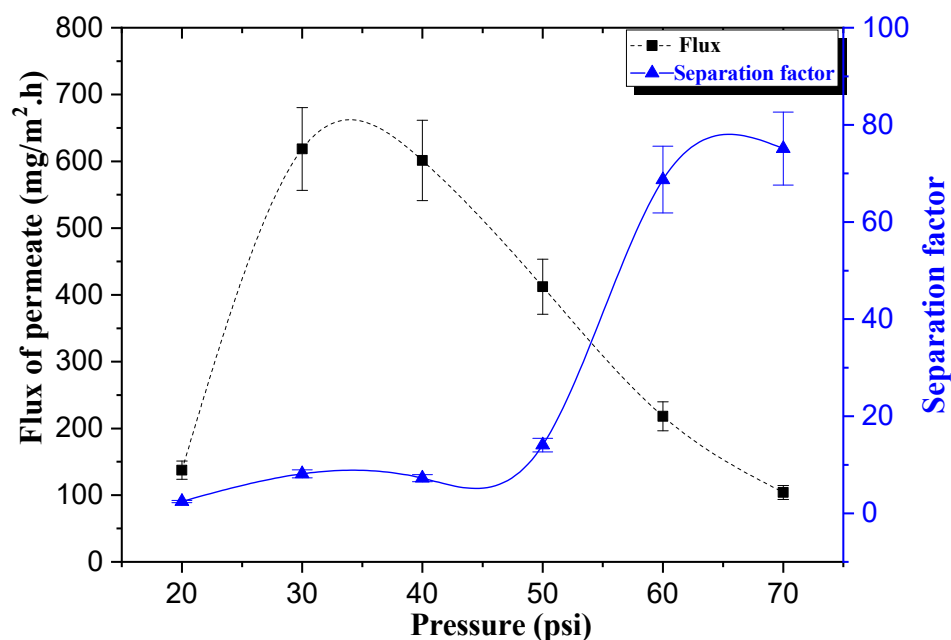
Figure 14. The flux of permeate and separation factor of the separation process of fermentation broth using poly (MMA-*co*-MA) membrane under different nitrogen pressures.

3.12.1. Plant Layout

Plant layout is the physical arrangement of the equipment and machines. The appropriate arrangement of equipment enhances the best performance and achieves the maximum benefit of heat and water recovery.

3.12.2. Equipment LIST

The major equipment and its uses are summarized in Table 3. For the reactors number calculations, the reactor can process around 150 tons of feedstock per batch, which takes 1 h for the pretreatment process. As per the design capacity of the plant, about 312 KTA of CS is required. The solution containing maleic acid would be 10 times the total feedstock, which is around 3.1 million tons. Therefore, the number of reactors should handle around 3.1 million tons of liquids. As a result, the number of required reactors for the pretreatment process will be around three reactors, as per the following calculations [52–54]:

Treated feedstock processed annually by one reactor	= mass of reactants per batch × number of periods × working days annually = 150 × 330 × 24 = 1,188,000 tons
Number of reactors required	= total amount of feedstock/(Treated corn processed annually by one reactor) = 3,120,000/(1,188,000) = 2.6

As per the design capacity of the plant, around 60% of this quantity (190 KTA) will remain after the pretreatment process and this will convert to glucose via enzymatic saccharification in the presence of the acetate buffer pH 5.0 solution. The buffer solution will be 20 times the remaining solid mass, thus the number of reactors should handle around 3.8 million tons of liquids. The reactor used in the enzymatic reaction can process around 150 tons per batch, which takes 4 days for the enzymatic reaction. Therefore, the number of reactors required will be 308 reactors, as per the following calculations:

Treated feedstock processed annually by one reactor	= mass of reactants per batch × number of periods/working days annually = 150 × (330/4) = 12,375 tons
Number of reactors required	= total amount of feedstock/(Treated corn processed annually by one reactor) = 3,800,000/(12,375) = 308

As per the calculations performed, the total number of reactors (150 tons capacity) will be 308 reactors and three reactors for the pretreatment process.

For tanks, the number of annual batches for the fermentation tanks is equal to 330/3 = 110 batches. Therefore, the number of tanks required will be as per the following calculations:

Feedstock fermented by one tank annually	= volume of reactants per batch × number of periods/working days annually = 150 × (330/3) = 16,500 tons
Number of tanks required	= total amount of feedstock/(Treated corn processed annually by one tank) = 3,800,000/(16,500) = 230 tanks

As per the calculations performed, the total number of tanks will be 230 tanks and 70 tanks for the other materials storage.

Table 3. Equipment list.

No.	Equipment	Uses
1	Plastic Tanks	Plastic tanks will be used for the enzymatic process, fermentation process, and the storage of feedstocks, methanol, distilled water, chemicals, and bioethanol.
2	Reactor	The reactors are usually cylindrical and with a vertical axis. The top of the reactor is closed to prevent air from entering the reaction.
3	Heat exchanger	The heat exchanger is used for heat recovery. Therefore, there will be two heat exchangers in service.
4	Pumps	The pump will be used to transfer the streams to the required destination.
5	Filters	The filters remove the solid biomass from the liquid after the enzymatic process. There will be 10 filters in the whole process.
6	Grinder	The grinder will be used to grind the feedstock to small particles.
7	Heaters	The heaters are used to heat the liquid to the required temperature. A thermal oil heater type is used in the study. There will be three heaters in the whole process, two in service, and one standby.

3.13. Process Description of the Bioethanol Production

The following section describes the bioethanol production process. Figure 15 is the process flow diagram that shows the process of bioethanol production, as per the following steps:

- The feedstock passes through a grinder for milling and sieving. The milled feedstock is pretreated in the reactor in order to react using a solution containing maleic acid (2%) at 120 °C, 45 psi for 1 h.
- In the enzymatic reactor, the biomass incubates with cellulase in the presence of the acetate buffer solution pH 5.0 at 50 °C for 4 days.

- The separated lignin and hemicellulose (a by-product from the enzymatic reactor) are stored in the crude lignin tank and sold for green power generation.
- The produced liquid phase of the glucose is oriented to the fermentation tank to be incubated with the yeast cells and some nutrients, such as potassium di-hydrogen phosphate, magnesium sulfate, and ammonium sulfate. This enhances the fermentation process for 3 days to produce bioethanol broth.
- For bioethanol purification, the produced bioethanol broth passes through heaters to raise the temperature. This enhances the bioethanol separation.
- The final purified bioethanol is withdrawn from the top of the evaporator and stored in the dedicated tanks.
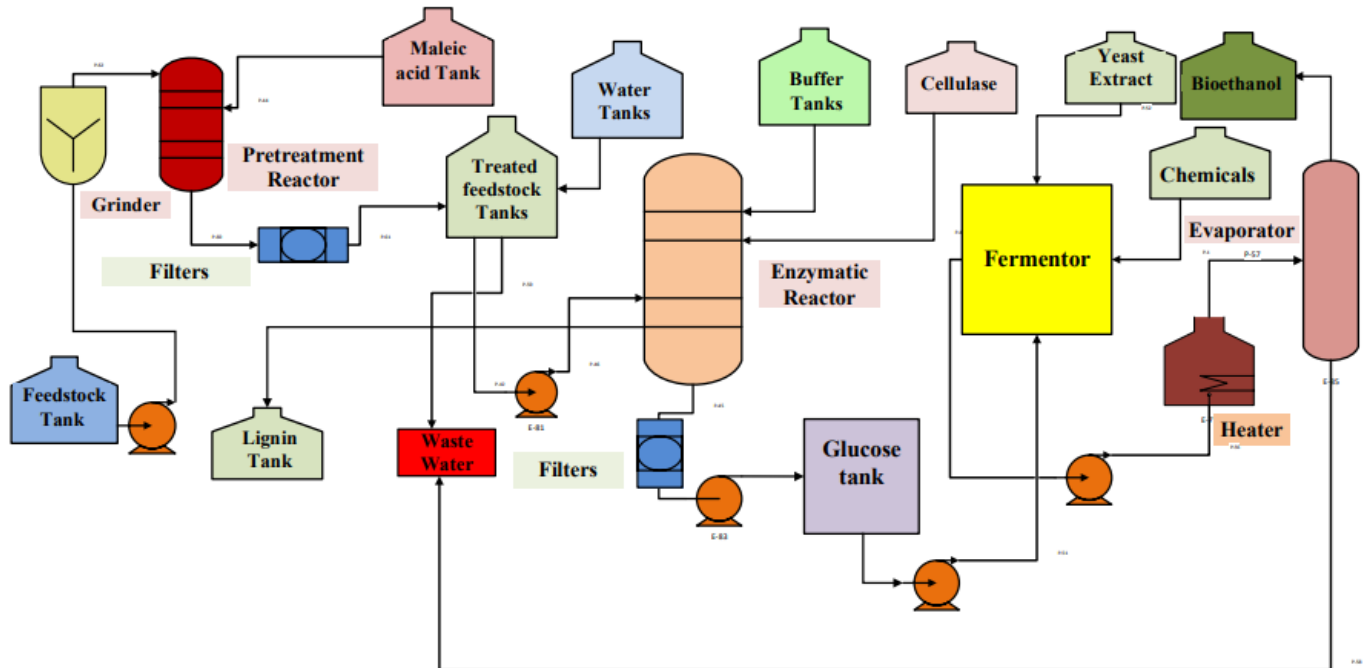
Figure 15. Process flow diagram of bioethanol production.

3.14. Design of Cost Estimation Model

The cost estimation model for the bioethanol production process was prepared using the Microsoft Excel program. The structure of the model was a series of sheets connected by mathematical equations. The connected sheets were as follows: The total capital investment sheet, the feedstocks and products prices sheet, the operating costs sheet, and the income statement sheet. The cost estimation model for the bioethanol production process was prepared using the Microsoft Excel program. The structure of the model was a series of sheets connected by mathematical equations. The connected sheets were as follows: The total capital investment sheet, the feedstocks and products prices sheet, the operating costs sheet, and the income statement sheet. The project finance did not include any loans or was loaded with debts, as the capital expenditure was not massive. The project cost was divided into two main categories: Capital expenditure and operating cost [55].

3.14.1. Capital Expenditure (CAPEX)

Capital costs are the expenses required to establish a project and purchase the fixed assets [56]. They are expensed once at the start of the project. CAPEX is categorized into purchased equipment cost (PEC) and the related PEC, as shown in Equation (13) [57]. The purchased equipment cost is the cost required to purchase the equipment used in the plant.

The related PEC is the cost corresponding to the plant build-up, such as instrumentation, installation, piping, and electrical [58].

$$CAPEX = PEC + related\ PEC \tag{13}$$

The purchased equipment cost (PEC) is the basis of the cost estimation model, and it should be precisely determined. The purchased equipment required for the bioethanol plant is stated in Table 4.

Table 4. The PEC in bioethanol production.

No.	Equipment	No.	Price/Unit	Price (USD)
1	Tanks (including storage and separator tanks)	300	1500	450,000
2	Evaporator	2	20,000	40,000
3	Heat exchanger	2	15,000	30,000
4	Pumps	5	5000	25,000
5	Filters	10	2000	20,000
7	Batched stirred reactor (150 tons)	311	10,000	3,110,000
8	Miller/grinder	3	8000	24,000
9	Heaters	3	20,000	60,000
	Total PEC: 3,609,000			

The costs of equipment installation, construction, transportation, and contingency can be estimated as a percentage of purchased equipment cost (PEC). This method is commonly used for the preliminary cost estimation of any project [59].

I.   Equipment installation cost

The cost of equipment installation involves costs for foundations, labor, construction expenses, supports, platforms, and any other factor that is directly related to the erection of purchased equipment. This usually averages 35% of the PEC for bioethanol plants [60].

II.   Instrumentation costs

Instrumentation costs include costs of installation, labor, instruments, and auxiliary devices and materials. The number of control devices required will determine the total instrumentation costs and may vary from 6 to 30% of the PEC. Generally, bioethanol plants do not require sophisticated control devices or instruments since flows are constant and all tanks have level indicators. Instrumentation costs will be estimated to be 20% of the purchased equipment cost [60].

III.   Piping costs

Piping costs include pipes, fittings, valves, labor, supports, and other items involved in the complete erection of all piping used in the process. The piping used in the process will be dedicated to distilled water, raw materials, intermediate products, and finished products. Piping costs for bioethanol plants were estimated at 36% of PEC for material and 30% of PEC for piping labor costs, thus the total cost of the piping is 66% of the PEC [60].

IV.   Electrical costs

Electrical costs include the costs of the electrical installation, power wiring, lighting, electrical transformations, and control devices. Power equipment requirements are relatively low for these plants; a factor of 11% of the purchased equipment cost (PEC) was considered for the electrical cost.

V.   Building and civil costs

The cost of buildings includes services, materials, foundations, and supplies involved in the erection of buildings. Services included in this cost are plumbing, heating, lighting,

ventilation, and similar building services. Building costs are equal to about 35% of the PEC for a new processing plant at a new site.

VI.　Transportation cost

Transportation cost covers all of the expenses required to transport the purchased equipment from its origin to the proposed plant location. Transportation costs are equal to about 15% of the PEC.

VII.　Contingency reserves cost

Contingency reserves address the cost impact of the risks, it covers unforeseen or risky events, and they will be 10% of the PEC. Table 5 shows the cost breakdown of the related PEC. Table 6 shows the total CAPEX for the bioethanol plant, calculated as per Equation (13).

Table 5. Related capital expenditure breakdown.

Item	Percentage	Price (USD)
Piping	0.66	897,250
Building	0.25	358,900
Civil	0.1	717,800
Instrumentation	0.2	394,790
Electrical	0.11	897,250
Installation	0.35	1,256,150
Soft cost (license fees, financing fees)	0.2	717,800
Transportation	0.15	538,350
Contingency	0.1	358,900
Total related PEC		7,651,080

Table 6. Total CAPEX.

Item	Value (USD Million)
PEC	3.6
Related PEC	7.6
Total CAPEX	11.2

3.14.2. Operating Expenditure (OPEX)

The optimum operating conditions achieved during the experimental trials are the basis of the economic indicators, particularly in the item of the OPEX. The reaction time, pressure, temperature, feed-in, output, etc., all these factors have a great reflection on the OPEX and economic study. Therefore, the optimization occurred only in the practical part and then the economic study is performed. Operating costs are the costs required yearly to operate the plant. OPEX is divided into fixed and variable costs [61].

Fixed costs are a fixed amount of money that is yearly expensed whether the plant is operated or not, such as maintenance, insurance, administration, depreciation, and tax costs. Depreciation represents the reduction in value of an asset. Table 7 shows the breakdown of fixed costs. The expected fixed costs until 2047 are shown in (Supplementary Materials Table S5). Although the depreciation cost is considered as a fixed cost, it is removed from the fixed cost table and placed in the income statement tables (Supplementary Materials Table S5).

Variable costs are yearly non-fixed expenses and vary at a rate directly related to the production of the plant. Variable costs are incurred only when the plant is in operation, such as raw materials, utilities, and chemicals [62]. Inflation is a sustained rise in the general price level of goods and services in an economy over a period of time and it is a constant rise in the general level of prices. Annual inflation is set for feedstock, raw material, chemicals, and products by 3%, but for labor and utilities by 4%.

Table 8 indicates the operating assumptions requirements for a plant capacity of 37 thousand tons per annum (KTA) of bioethanol. The prices of raw materials were obtained from pricing reports or local market suppliers.

Table 7. Fixed cost breakdown.

Item	Percentage of PIC
Maintenance	10
Insurance	3
Administration	15
Depreciation	10

Table 8. Raw materials that are required for a 50 KTA of bioethanol production.

Item	KTA
Input products	
Corn feedstock	312.5
Remaining Solid Mass	190
Malic acid	31.3
Cellulase	50.7
S. Cerevisiae cells	22.1
Acetic Acid	28.4
Sodium Acetate	9.5
Potassium dihydrogen phosphate (KH2PO4)	1.9
Ammonium sulfate	9.5
Magnesium sulfate	0.9
Yeast extract	1.9
Output products	
Lignin	79
Bioethanol Yield	37.5

The ton price of feedstock, raw materials, and bioethanol until 2047 are shown in (Supplementary Materials Table S7). The total feedstock and raw material costs required to produce 37 KTA of bioethanol until 2047 are shown in (Supplementary Materials Table S8).

In this project, the utilities include water, fuel, and electricity. The prices of utilities are obtained from other projects executed in Egypt. For the fuel gas consumption, the heater as per its datasheet consumes approximately 80 m^3 of fuel gas per ton of bioethanol. Water consumption is estimated to be 10 tons per ton of bioethanol. Electricity consumption is 1000 Kw/h per ton of bioethanol. Chemicals for washing and cleaning are considered a variable cost and their cost are around USD 200 thousand in the first year with an annual inflation rate of 3% [60]. The retail prices of each utility until 2047 are indicated in (Supplementary Materials Table S9) and the total utilities costs until 2047 are shown in (Supplementary Materials Table S8).

Direct labor is estimated to be 100 employees. The average salary will be USD 1500/month for each employee with an annual inflation rate of 4%. The labor costs expected until 2047 are shown in (Supplementary Materials Table S10).

3.15. Project Indicators

The project's revenue is determined as per Equation (14) [63]:

$$\text{Project revenue} = (\text{Price of bioethanol ton} \times \text{the total production of bioethanol}) + (\text{Price of lignin ton} \times \text{total production of the lignin}) \tag{14}$$

The production capacity varies according to the process type of bioethanol production. In the cost estimation model, the bioethanol price is considered as USD 900/ton with an annual inflation rate of 3%. The project revenue is not the only factor to detect the project feasibility. Gross and net profit are also important factors to decide the project profitability

and they are determined as per Equations (15) and (16) [53]. Gross profit and net profit appear in the last lines of the income statement sheet [63]:

$$\text{Gross profit} = \text{Revenue} - \text{OPEX} \tag{15}$$

$$\text{Net profit} = \text{Gross profit} - \text{Depreciation} - \text{taxes} \tag{16}$$

The income statement is a sheet used to evaluate the project profitability as it summarizes the revenues, expenses, total operating cost, taxes, and gross profit for the project period. The estimated rate of taxes is 20% of the gross profit. The income statement shows that the bioethanol process achieves a considerable profit for the whole duration of the project without any losses as it achieves a net profit of USD 1 million in 2023, reaching USD 2.1 million in 2047. The net profit is mentioned in the income sheet (Supplementary Materials Table S6) and expressed in Figure 16.
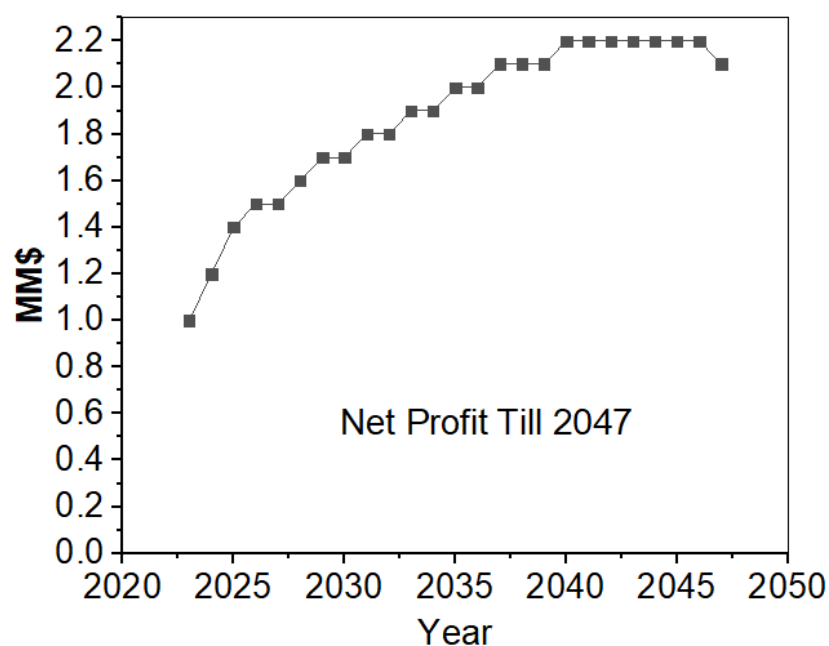
Figure 16. Net profit for bioethanol plant.

It is evident that there is a gradual increase in the net profit until 2042 by USD 2.2 million, then there will be a decrease in the net profit (Figure 14) due to the fact that the increased rate of OPEX exceeds the increased rate of revenues, but generally, there is still considerable net profit.

Net present value (NPV) is the difference between the present value of cash inflows and the present value of cash outflows over a period. NPV is used to analyze the profitability of a project. Positive NPV indicates that the project is profitable, while negative NPV indicates that the project achieves losses. Table 8 shows that the bioethanol project will achieve a positive NPV of USD 3.35 million, thus the project is feasible.

The term payback period refers to the time required to recover the cost of the capital expenditure (CAPEX). The shorter payback a project has, the more feasible it is. Therefore, the payback period is useful for expecting the feasibility of the project and calculated by dividing the initial CAPEX by the average net cash flows. Table 9 shows that the payback period is 8 years, which is considered a short time, proving that bioethanol is an attractive project.

Internal rate of return (IRR) is a method of calculating an investment rate of return and it is an indicator of the efficiency or quality of a project. Table 9 shows that IRR is 13%, which is greater than the minimum required rate of return in Egypt (7.5%), proving that bioethanol is a very profitable project.

Table 9. Bioethanol project indicators.

NPV (USD million)	3.35
Payback (years)	8
IRR	13%

3.16. Practical Implications

For most African countries, increasing demand and identifying energy supplies are major concerns. The Egyptian government is cognizant of the need for sustainable energy to address the increasing energy demand, and to move to a more environmentally sustainable one. The 2035 Integrated Sustainable Energy Strategy, which builds on previous strategies, emphasizes the importance of using renewable energy sources as alternative and sustainable sources of energy. Egypt is working on increasing the supply of electricity generated from renewable sources to 20% by 2022 and 42% by 2035 [64]. In addition, the country is highly vulnerable to oil price shocks as it imports almost 101.12 thousand barrels per day of oil from Egypt in February 2022 [65]. The challenges of the restricted and unstable energy access and excess biomass wastes have led to practical implications in Egypt with a focus on energy consumption management and the search for alternative sources of biofuel, which are astringent necessities to meet the energy demands and reduce greenhouse gas (GHG) emissions [66].

4. Conclusions

The current study focuses on the optimum bioconversion of CS as an agricultural waste into bioethanol using the maleic acid pretreatment under autoclaving conditions. The optimum operating conditions of the physico-chemical pretreatment were a 2% maleic acid concentration, 1:20 solid-to-liquid ratio, at 120 °C for 1 h of operation in the autoclave. The pretreatment process contributed to 52.8 and 45.2% lignin and hemicellulose removal and contributed to 98.15% cellulose recovery. The data from proximate, ultimate, and thermal analysis found that the CSM exhibits higher physico-chemical properties than CS and the other biomasses reported in the literature. Cellulase enzyme from Trichoderma reesei ($\geq$700 U/g) efficiently converted the recovered cellulose to glucose (741 mg/dL) under the conditions of 2% CSM in 10 mL acetate buffer (pH 5.5) and 100 µL cellulase concentration at 50 °C and shaking speed of 150 rpm for 72 h of incubation period. The fermentation process was performed using a yeast strain isolated from rotten apple juice that succeeded in the production of a high bioethanol concentration of (1230 mg/dL) under anaerobic conditions, pH value of 5, and 5% inoculum size at 30 °C. This isolated yeast strain was close to *Pichia nakasei* with a similarity of 98%, and its amplified 18S rRNA gene sequence was deposited in GenBank with the accession number MZ675535. Poly (MMA-*co*-MA) membrane was synthesized, characterized, and utilized in bioethanol purification via a pervaporation system at different nitrogen pressures. Poly (MMA-*co*-MA) membrane led to raising the bioethanol concentration in the fermentation broth from 30 to 76.33%, indicating that the synthesized poly (MMA-*co*-MA) membrane is a hydrophobic membrane with high selectivity for ethanol than water. These results revealed the high efficiency of the utilized pervaporation system and the synthesized poly (MMA-*co*-MA) membrane in the bioethanol separation and purification. The economic study predicts that the total CAPEX will be USD 11.2 million, and there will be a gradual increase in the net profit until 2042 by USD 2.2 million, then the net profit will be lessened, but it is still a considerable profit. The total net profit gained from this bioethanol project during the whole project life will be USD 35 million. The NPV of the project will be USD 3.35 million, which indicates a feasible project. The project payback period is 8 years, which proves the attractiveness of the bioethanol project as it will retain the investment cost within a short period. The project IRR is 13%, indicating that bioethanol is a very profitable project. Eventually, the economic assessment reveals that the bioethanol production from CS using this technique represents a promising sequential strategy and excellent adaptability for high bioethanol production that makes a worthy net profit during the whole project duration without achieving any

losses. The project indicators, such as NPV, payback, and IRR found that bioethanol is a very promising project and enhances project profitability.

It is recommended for further research to implement this strategy of bioethanol production on other types of low-cost agricultural wastes, such as rice straw, in order to add value to these wastes and prevent many health and environmental hazards from occurring due to its incorrect disposal and burning in open areas.

References

1. Ahmad, A.; Ismail, S.; Ahmad, I.; Adamu, I.; Jakada, A.; Farouq, I.; Mustapha, U.; Muhammad, U.; Abdullahi, A.; Fagge, A.; et al. Pollutant emissions, renewable energy consumption and economic growth: An empirical review from 2015–2019. *J. Environ. Treat. Tech.* **2020**, *8*, 323–335.
2. Salleh, S.; Gunawan, M.; Bin Zulkarnain, M.; Shamsuddin, A.; Abdullah, T. Modelling and optimization of biomass supply chain for bioenergy production. *J. Environ. Treat. Tech.* **2019**, *7*, 689–695.
3. Bušić, A.; Marđetko, N.; Kundas, S.; Morzak, G.; Belskaya, H.; Šantek, M.; Komes, D.; Novak, S.; Šantek, B. Bioethanol production from renewable raw materials and its separation and purification: A review. *Food Technol. Biotechnol.* **2018**, *56*, 289–311. [CrossRef]
4. Independent Statistics and Analysis, U.S. Energy Information and Administration, Biofuel Explained, Ethanol and Environment. Available online: www.eia.gov/todayinenergy/details.php?id=52380 (accessed on 20 May 2022).
5. Jeswani, H.K.; Chilvers, A.; Azapagic, A. Environmental sustainability of biofuels: A review. *Proc. R. Soc. A* **2020**, *476*, 20200351. [CrossRef]

6. Elyamny, S.; Hamdy, A.; Ali, R.; Hamad, H. Role of combined Na_2HPO_4 and $ZnCl_2$ in the unprecedented catalysis of the sequential pretreatment of sustainable agricultural and agro-industrial wastes in boosting bioethanol production. *Int. J. Mol. Sci.* **2022**, *23*, 1777. [CrossRef]

7. Hassan, M.; Chowdhury, R.; Ghosh, S.; Manna, D.; Pappinen, A.; Kuittinen, S. Energy and environmental impact assessment of Indian rice straw for the production of second-generation bioethanol. *Sustain. Energy Technol. Assess.* **2021**, *47*, 101546. [CrossRef]

8. Behera, S.; Arora, R.; Nandhagopal, N.; Kumar, S. Importance of chemical pretreatment for bioconversion of lignocellulosic biomass. *Renew. Sustain. Energy Rev.* **2014**, *36*, 91–106. [CrossRef]

9. Chen, M.; Zhao, J.; Xia, L. Comparison of four different chemical pretreatments of corn stover for enhancing enzymatic digestibility. *Biomass Bioenergy* **2009**, *33*, 1381–1385. [CrossRef]

10. Tan, H.; Yang, R.; Sun, W.; Wang, S. Peroxide-acetic acid pretreatment to remove bagasse lignin prior to enzymatic hydrolysis. *Ind. Eng. Chem. Res.* **2010**, *49*, 1473–1479. [CrossRef]

11. Hsu, T.-C.; Guo, G.-L.; Chen, W.-H.; Hwang, W.-S. Effect of dilute acid pretreatment of rice straw on structural properties and enzymatic hydrolysis. *Bioresour. Technol.* **2010**, *101*, 4907–4913. [CrossRef]

12. Hamdy, A.; Abd Elhafez, S.; Hamad, H.; Ali, R. The Interplay of Autoclaving with Oxalate as Pretreatment Technique in the View of Bioethanol Production Based on Corn Stover. *Polymers* **2021**, *13*, 3762. [CrossRef]

13. Kootstra, A.M.J.; Beeftink, H.H.; Scott, E.L.; Sanders, J.P.M. Comparison of dilute mineral and organic acid pretreatment for enzymatic hydrolysis of wheat straw. *Biochem. Eng. J.* **2009**, *46*, 126–131. [CrossRef]

14. Qin, L.; Liu, Z.; Li, B.; Dale, B.; Yuan, Y. Bioresource Technology Mass balance and transformation of corn stover by pretreatment with different dilute organic acids. *Bioresour. Technol.* **2012**, *112*, 319–326. [CrossRef]

15. Yan, Y.; Zhang, C.; Lin, Q.; Wang, X.; Cheng, B.; Li, H.; Ren, J. Microwave-Assisted Oxalic Acid Pretreatment for the Enhancing of Enzyme Hydrolysis in the Production of Xylose and Arabinose from Bagasse. *Molecules* **2018**, *23*, 862. [CrossRef]

16. Chai, L.; Li, H.; Zheng, X.; Wang, J.; Yang, J.; Lu, J.; Yin, D.; Zhang, Y. Pervaporation separation of ethanol–Water mixtures through B-ZSM-11 zeolite membranes on macroporous supports. *J. Membr. Sci.* **2015**, *491*, 168–175. [CrossRef]

17. Zentou, H.; Abidin, Z.; Yunus, R.; Biak, D.; Issa, M.; Pudza, M. Modelling of mass transfer during pervaporation of ethanol/water mixture using polydimethylsiloxane membrane. *Chem. Eng. Res. Des.* **2021**, *175*, 320–329. [CrossRef]

18. Liu, Q.; Li, Y.; Li, Q.; Liu, G.; Liu, G.; Jin, W. Mixed-matrix hollow fiber composite membranes comprising of PEBA and MOF for pervaporation separation of ethanol/water mixtures. *Sep. Purif. Technol.* **2019**, *214*, 2–10. [CrossRef]

19. Ranjithkumar, M.; Uthandi, S.; Kumar, P.; Muniraj, I.; Thanabal, V.; Rajarathinam, R. Highly crystalline cotton spinning wastes utilization: Pretreatment, optimized hydrolysis and fermentation using Pleurotus florida for bioethanol production. *Fuel* **2022**, *308*, 122052. [CrossRef]

20. Singh, Y.; Mahanta, P.; Bora, U. Comprehensive characterization of lignocellulosic biomass through proximate, ultimate and compositional analysis for bioenergy production. *Renew. Energy* **2017**, *103*, 490–500. [CrossRef]

21. Demirbas, A. Combustion characteristics of different biomass fuels. *Prog. Energy Combust. Sci.* **2004**, *30*, 216–230. [CrossRef]

22. Srivastava, H.; Lade, H.; Paul, D.; Arthanareeswaran, G.; Kweon, J. Styrene-based copolymer for polymer membrane modifications. *Appl. Sci.* **2016**, *6*, 159. [CrossRef]

23. Lyu, Q.; Chen, X.; Zhang, Y.; Yu, H.; Han, L.; Xiao, W. One-pot fractionation of corn stover with peracetic acid and maleic acid. *Bioresour. Technol.* **2021**, *320*, 124306. [CrossRef]

24. Prasad, B.; Padhi, R.; Ghosh, G. A review on key pretreatment approaches for lignocellulosic biomass to produce biofuel and value-added products. *Int. J. Environ. Sci. Technol.* **2022**. [CrossRef]

25. Yusuf, A.; Inambao, F. Characterization of Ugandan biomass wastes as the potential candidates towards bioenergy production. *Renew. Sustain. Energy Rev.* **2020**, *117*, 109477. [CrossRef]

26. Hossain, M.A.; Ganesan, P.B.; Sandaran, S.C.; Rozali, S.B.; Krishnasamy, S. Catalytic microwave pyrolysis of oil palm fiber (OPF) for the biochar production. *Environ. Sci. Pollut. Res.* **2017**, *24*, 26521–26533. [CrossRef]

27. Saldarriaga, J.F.; Aguado, R.; Pablos, A.; Amutio, M.; Olazar, M.; Bilbao, J. Fast characterization of biomass fuels by thermogravimetric analysis (TGA). *Fuel* **2015**, *140*, 744–751. [CrossRef]

28. Nizamuddin, S.; Baloch, H.; Siddiqui, M.; Mubarak, N.; Tunio, M.; Bhutto, A.; Jatoi, A.; Griffin, G.; Srinivasan, M. An overview of microwave hydrothermal carbonization and microwave pyrolysis of biomass. *Rev. Environ. Sci. Biotechnol.* **2018**, *17*, 813–837. [CrossRef]

29. Makul, N.; Fediuk, R.; Amran, M.; Al-Akwaa, M.; Pralat, K.; Nemova, D.; Petropavlovskii, K.; Novichenkova, T.; Petropavlovskaya, V.; Sulman, M. Utilization of Biomass to Ash: An Overview of the Potential Resources for Alternative Energy. *Materials* **2021**, *14*, 6482. [CrossRef]

30. Hassaan, M.A.; Hosny, S.; ElKatory, M.R.; Ali, R.M.; Rangreeze, T.A.; El Nemr, A. Dual action of both green and chemically synthesized zinc oxide nanoparticles: Antibacterial activity and removal of Congo red dye. *Desalin. Water Treat.* **2021**, *218*, 423–435. [CrossRef]

31. Elkatory, M.; Soliman, E.; Hassaan, M.; Ali, R.; Hafez, E.; Ibrahim, H.S.; Hashem, A. Chemical mitigation technology for wax deposition in submarine oil pipeline systems. *Egypt. J. Chem.* **2021**, *64*, 5989–5997. [CrossRef]

32. Bassyouni, D.; Mohamed, M.E.; El-Ashtoukhy, E.; Abd El-Latif, M.; Zaatout, A.; Hamad, H. Fabrication and characterization of electrospun Fe_3O_4/o-MWCNTs/polyamide 6 hybrid nanofibrous membrane composite as an efficient and recoverable adsorbent for removal of Pb (II). *Microchem. J.* **2019**, *149*, 103998. [CrossRef]

33. Eltarahony, M.; Abu-Serie, M.; Hamad, H.; Zaki, S.; Abd-El-Haleem, D. Unveiling the role of novel biogenic functionalized CuFe hybrid nanocomposites in boosting anticancer, antimicrobial and biosorption activities. *Sci. Rep.* **2021**, *11*, 7790. [CrossRef]

34. Liu, Y.; Chen, W.; Xia, Q.; Guo, B.; Wang, Q.; Liu, S.; Liu, Y.; Li, J.; Yu, H. Efficient cleavage of lignin–carbohydrate complexes and ultrafast extraction of lignin oligomers from wood biomass by microwave-assisted treatment with deep eutectic solvent. *Chem. Sus. Chem.* **2017**, *10*, 1692–1700. [CrossRef]

35. Scelsi, E.; Angelini, A.; Pastore, C. Deep eutectic solvents for the valorisation of lignocellulosic biomasses towards fine chemicals. *Biomass* **2021**, *1*, 29–59. [CrossRef]

36. Banoth, C.; Sunkar, B.; Tondamanati, P.R.; Bhukya, B. Improved physicochemical pretreatment and enzymatic hydrolysis of rice straw for bioethanol production by yeast fermentation. *3 Biotech* **2017**, *7*, 334. [CrossRef]

37. Singh, R.; Shukla, A.; Tiwari, S.; Monika Srivastava, M. A review on delignification of lignocellulosic biomass for enhancement of ethanol production potential. *Renew. Sust. Energ. Rev.* **2014**, *32*, 713–728. [CrossRef]

38. Kham, L.; Le Bigot, Y.; Delmas, M.; Avignon, G. Delignification of wheat straw using a mixture of carboxylic acids and peroxoacids. *Ind. Crop. Prod.* **2005**, *21*, 9–15. [CrossRef]

39. Saifuddin, N.; Refal, H. Optimization of fermentation parameters for bioethanol production from waste glycerol by microwave induced mutant Escherichia coli. *Res. J. Pharm. Biol. Chem. Sci.* **2015**, *6*, 1449–1461.

40. Periyasamy, S.; Venkatachalam, S.; Ramasamy, S.; Srinivasan, V. Production of bio-ethanol from sugar molasses using Saccharomyces cerevisiae. *Mod. Appl. Sci.* **2009**, *3*, 32–37. [CrossRef]

41. Wong, Y.; Sanggari, V. Bioethanol production from sugarcane bagasse using fermentation process. *Orient. J. Chem.* **2014**, *30*, 507–513. [CrossRef]

42. Hassaan, M.A.; Pantelo, A.; Luigi, T.; Elkatory, M.R.; Ali, R.M.; El Nemr, A. Enhancement of biogas production via green ZnO nanoparticles: Experimental results of selected herbaceous crops. *Chem. Eng. Commun.* **2021**, *208*, 242–255. [CrossRef]

43. Hamadi, A.; Yeddou-Mezenner, N.; Azeddine, L.; Ali, R.M.; Hamd, H. Upgrading of agro-industrial green biomass residues from chocolate industry for adsorption process: Diffusion and mechanistic insights. *J. Food Sci. Technol.* **2021**, *58*, 1081–1092. [CrossRef]

44. Ali, R.M.; Hamad, H.A.; Hussein, M.M.; Malash, G.F. Potential of using green adsorbent of heavy metal removal from aqueous solutions: Adsorption kinetics, isotherm, thermodynamic, mechanism and economic analysis. *Ecol. Eng.* **2016**, *91*, 317–332. [CrossRef]

45. Kamel, D.A.; Farag, H.A.; Amin, N.K.; Zaatout, A.A.; Ali, R.M. Smart utilization of Jatropha (*Jatropha curcas* Linnaeus) seeds for biodiesel production: Optimization and mechanism. *Ind. Crop. Prod.* **2018**, *111*, 407–413. [CrossRef]

46. Sindhu, K.P.; Abdul Majeed, S.S.M.; Shahitha Parveen, J. PEO/PMMA Solid Nanocomposite Polyelectrolyte with Enhanced Ionic Conductivity and Promising Dielectric Properties. *J. Electron. Mater.* **2021**, *50*, 6654–6666. [CrossRef]

47. Ali, R.M.; Hassaan, M.A.; Elkatory, M.R. Towards potential removal of malachite green from wastewater: Adsorption process optimization and prediction. *MSF* **2020**, *1008*, 213–221. [CrossRef]

48. Eldin, M.M.; Elaassar, M.; Elzatahry, A.; Al-Sabah, M. Poly (acrylonitrile-co-methyl methacrylate) nanoparticles: I. Preparation and characterization. *Arab. J. Chem.* **2017**, *10*, 1153–1166.

49. Rao, M.; Liu, J.; Li, W.; Liang, Y.; Liao, Y.; Zhao, L. Performance improvement of poly (acrylonitrile-vinyl acetate) by activation of poly (methyl methacrylate). *J. Power Source* **2009**, *189*, 711–715. [CrossRef]

50. Rahimalimamaghani, A.; Tanaka, D.; Tanco, M.; D'Angelo, F.; Gallucc, F. New hydrophilic carbon molecular sieve membranes for bioethanol dehydration via pervaporation. *Chem. Eng. J.* **2022**, *435*, 134891. [CrossRef]

51. Abu-Saied, M.; Taha, T.H.; Elnaggar, E.M.; Amer, R.A.; Mansy, A.; Elkady, G.M. Green production of bio-ethanol from cellulosic fiber waste and its separation using polyacrylonitrile-co-poly methyl acrylate membrane. *Cellulose* **2018**, *25*, 6621–6644. [CrossRef]

52. De Paola, M.G.; Mazza, I.; Paletta, R.; Lopresto, C.G.; Calabrò, V. Small-Scale Biodiesel Production Plants—An Overview. *Energies* **2021**, *14*, 1901. [CrossRef]

53. Elgharbawy, A.S.; Sadik, W.A.; Sadek, O.M.; Kasaby, M.A. Glycerolysis treatment to enhance biodiesel production from low-quality feedstocks. *Fuel* **2021**, *284*, 118970. [CrossRef]

54. Elgharbawy, A.S.; Sadik, W.A.; Sadek, O.M.; Kasaby, M.A. Maximizing biodiesel production from high free fatty acids feedstocks through glycerolysis treatment. *Biomass Bioenergy* **2021**, *146*, 105997. [CrossRef]

55. Elgharbawy, A.; Sayed, A. A review on natural gas previous, current and forecasting prices and demand. *JPME* **2020**, *22*, 61–64. [CrossRef]

56. Deo, P. Fixed Asset Management-Revisited. *J. Account. Finance* **2021**, *21*, 2158–3625.

57. Cano, P.I.; Colon, J.; Ramirez, M.; Lafuente, J.; Gabriel, D.; Cantero, D. Life cycle assessment of different physical-chemical and biological technologies for biogas desulfurization in sewage treatment plants. *J. Clean Prod.* **2018**, *181*, 663–674. [CrossRef]

58. Santana, G.; Martins, P.; Da Silva, N.D.L.; Batistella, C.; Maciel Filho, R.; Maciel, M.W. Simulation and cost estimate for biodiesel production using castor oil. *Chem. Eng. Res. Des.* **2010**, *88*, 626–632. [CrossRef]

59. Yuan, T.; Xiang, P.; Li, H.; Zhang, L. Identification of the main risks for international rail construction projects based on the effects of cost-estimating risks. *J. Clean Prod.* **2020**, *274*, 122904. [CrossRef]

60. Streimikiene, D.; Baležentis, T.; Baležentienė, L. Comparative assessment of road transport technologies. *Renew. Sustain. Energy Rev.* **2013**, *20*, 611–618. [CrossRef]

61. Ioannou, A.; Angus, A.; Brennan, F. Stochastic prediction of offshore wind farm LCOE through an integrated cost model. *Energy Procedia* **2017**, *107*, 383–389. [CrossRef]

62. Gnanaprakasam, A.; Sivakumar, V.M.; Surendhar, A.; Thirumarimurugan, M.; Kannadasan, T. Recent strategy of biodiesel production from waste cooking oil and process influencing parameters: A review. *J. Energy* **2013**, *2013*, 926392. [CrossRef]
63. Campbell, R.M.; Anderson, N.M.; Daugaard, D.E.; Naughton, H.T. Financial viability of biofuel and biochar production from forest biomass in the face of market price volatility and uncertainty. *Appl. Energy* **2018**, *230*, 330–343. [CrossRef]
64. Available online: https://www.trade.gov/country-commercial-guides/egypt-renewable-energy (accessed on 15 May 2022).
65. Available online: https://knoema.com/atlas/Egypt/topics/Energy/Oil/Exports-of-crude-oil (accessed on 15 May 2022).
66. Yusuf, A.A.; Inambao, F.L. Progress in alcohol-gasoline blends and their effects on the performance and emissions in SI engines under different operating conditions. *Int. J. Ambient Energy* **2018**, *42*, 465–481. [CrossRef]